Title
X-RAY PHOTOELECTRON SPECTROSCOPY: A TOOL FOR RESEARCH IN CATALYSIS

Authors
Delgass, W. Nicholas
Hughes, Thomas R.
Fadley, Charles S.

Publication Date
1970-02-01

Submitted to Catalysis Reviews

UCRL-18968
Preprint

c.2

X-RAY PHOTOELECTRON SPECTROSCOPY: A TOOL FOR RESEARCH IN CATALYSIS

W. Nicholas Delgass, Thomas R. Hughes, Charles S. Fadley

February 1970

AEC Contract No. W-7405-eng-48

UCRL-18968

DISCLAIMER

Submitted to Catalysis Reviews

X-RAY PHOTOELECTRON SPECTROSCOPY: A TOOL FOR RESEARCH IN CATALYSIS

W. Nicholas Delgass,[a,c] Thomas R. Hughes,[b] Charles S. Fadley[a,d]

a.Department of Chemistry and The Lawrence Radiation Laboratory, University of California, Berkeley

b.Chevron Research Company, Richmond, California

c. Present address: Department of Engineering and Applied Science, Yale University, New Haven, Connecticut 06520

d.Present address: Physics Department, Chalmers University of Technology, Gothenburg, Sweden

I. INTRODUCTION

Over the last ten years, a new technique for measuring electron binding energies has been developed by Siegbahn and co-workers at Uppsala (1). The method, now variously called electron spectroscopy for chemical analysis (ESCA), x-ray photoelectron spectroscopy (XPS), or induced electron emission (IEE), has stimulated the interest of researchers in several fields. By virtue of the semi-surface nature of the measurement on solids and the relation of shifts in photoelectron line positions to the chemical state of the atoms under study, this technique represents a new tool with high potential for catalytic research.

In an XPS experiment photoelectrons are ejected from the sample by x-ray excitation (See Figure 6). The kinetic energy of the ejected electrons is analyzed and peaks in the resulting kinetic energy spectrum correspond to electrons of specific binding energies in the sample. Of the many interesting results already produced by XPS, a few are summarized here to illustrate some of the characteristics of the technique. Chemical shifts in photoelectron line positions and, therefore, in the electron binding energies are of prime importance. The carbon (1s) (see (1) for the relation between chemical and x-ray notations for energy levels) spectrum of ethyltriflouroacetic acid (1, p. 21)

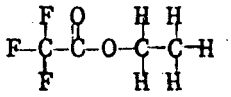

nicely demonstrates such shifts. The four chemically different carbon atoms produce a four line spectrum with a shift of nearly 9eV between the methyl and trifluoro carbon atoms. The spectrum also shows that

more electronegative ligands increase the binding energy of electrons on the central atom. Many correlations between chemical shifts and calculated charges on atoms have been drawn. An example for nitrogen is shown in Figure 1(2). The charges were calculated by the complete neglect of differential overlap (CNDO) molecular orbital method. The compounds corresponding to the numbers on the correlation diagram are given in Table 1.

Another study presented in reference (1) demonstrates the sensitivity of the XPS technique to monolayer surface coverages. Figure 2 shows the I($3d_{5/2}$) lines from 1, 3, and 10 double layers of iodostearic acid on a chromium-plated surface. From the saturation of the intensity of the iodine line, Siegbahn et al. estimated a mean escape depth of less than 100 Å for the I($3d_{5/2}$) photoelectrons. Thus, while studies of monolayers are possible, the photoelectron spectrum of a solid normally reflects the characteristics of a surface layer several atoms thick.

Although most of the discussion in this paper will be devoted to studies of core electrons, it should be noted that studies of outer electrons can also be carried out with x-ray photoelectron spectroscopy. Siegbahn et al. (1) have shown that for simple molecules, such as benzene, molecular orbital structure can be elucidated. Densities of states for valence bands in solids can also be determined (3).

Reference (3) contains, in addition, a study of the reduction of the surface oxide on an iron foil (Figure 3). The double line from the Fe (3p) level at 25°C shows that photoelectrons escape from both

Table 1

Identification of Nitrogen Compounds in Figure 1

1.	$NaNO_3$	6.	KCN	11.	$N_2H_6SO_4$	16.	$(CONH_2)_2$
2.	$NaNO_2$	7.	KOCN	12.	$(CH_3)_3NO$	17.	$(NH_2)_2CNCN$
3.	$Na[ONNO_2]$	8.	p-$HOC_6H_4NO_2$	13.	NH_4NO_3	18.	C_6H_5CN
4.	NaNNN	9.	$C_6H_5NO_2$	14.	$(CH_3)_4NB_3H_8$	19.	C_5H_5N
5.	NaN_2O_2	10.	n-$C_5H_{11}ONO$	15.	NH_3OHCl		

the oxide layer and the metal beneath it. The line corresponding to oxidized Fe falls to the left of the Fe metal line. This corresponds to higher electron binding energy or lower kinetic energy, as shown on the abscissa of Figure 3. As the temperature of the iron foil was raised in a flow of H_2 at ca. 10^{-2}torr, the reduction of the surface oxide layer was demonstrated by the disappearance of the left peak. A corresponding decrease in the intensity of the O (1s) line was found. Fadley and Shirley suggest that the shoulder on the O (1s) line at 25°C may be due to adsorbed, oxygen-containing gases.

Quantitative analysis from x-ray photoelectron spectra is demonstrated in Figure 4. The ratio of Si (2p) to Al (2p) peak areas for Y zeolite, divided by that ratio for mordenite, gives an experimental value of 0.48. The value calculated from known Si/Al ratios for the samples is 0.47.

We have been fortunate to have had the opportunity to further explore the potential of x-ray photoelectron spectroscopy for studies in catalysis and will present our findings here. The paper is divided into four major sections: 1) a review of the fundamentals of XPS; 2) comments on experimental equipment required; 3) experimental results on systems of catalytic interest; and finally, 4) some concluding remarks on the general applicability of x-ray photoelectron spectroscopy to catalysis.

II. FUNDAMENTALS

A. Overview

In electron spectroscopy, bound electrons are ejected from solids or gases by means of monoenergetic x-ray or ultraviolet photons or by electron impact. Two important types of electrons are ejected. The first type is photoelectrons ejected directly from bound electronic energy levels. The kinetic energy of the photoelectrons depends on both the energy of the exciting radiation and the electron binding energy. The second type results from Auger processes following ejection of an electron from an inner shell. The vacancy is filled by an electron from an outer shell, and the energy released is transferred to another outer electron which leaves the atom as an Auger electron. The kinetic energy of an Auger electron is independent of the primary radiation and depends only on the energy levels of the electronic states involved. Ultraviolet radiation has been used for studies of gases (4), densities of states in solids (5), and adsorbed species (6). Many Auger electron studies of solids (7) and some on gases (1,8) have also been reported. In this paper, we consider primarily photoelectrons excited from core levels by x-radiation, since these electrons directly reflect the charge distribution in the sample.

The principle of x-ray photoelectron spectroscopy is straightforward. X-rays incident on the sample cause the ejection of photoelectrons whose kinetic energy is then measured with high precision. A plot of the number of electrons detected versus the electron kinetic energy is the photoelectron spectrum. The binding energy of the electrons

is calculated from the energy of the x-ray photon and the kinetic energy of the electrons which escape from the sample without significant energy loss. Shifts in the binding energy reflect the chemistry of the atoms under study. Since the chemical shifts are of the order of a few eV, the photoelectron peaks can usually be assigned to the electron levels of origin by comparison with tabulated electron binding energies. In addition, the areas of the primary peaks in a photoelectron spectrum are proportional to the product of the photoelectric cross section per atom and the number of atoms producing photoelectrons which escape from the sample without significant energy loss. With calibration or prior knowledge of cross sections, peak areas can, therefore, yield quantitative chemical analysis of a low-pressure, gaseous sample. Quantitative analysis of solids by this method is more difficult because photoelectrons escape without energy loss only from a layer near the surface and photoelectrons of different energies may penetrate the sample to different extents. Thus, the peak areas yield the bulk composition only if the sample is homogeneous.

In principle, then, XPS offers the following features: a) sensitivity to nearly all elements; b) ability to study samples in gas, solid, and in some cases, liquid phases; c) determination of chemical effects related to the electronic charge distribution within the sample; and, d) a qualified chemical analysis of the effective sample composition.

B. Interpretation of Data

The first step in the interpretation of a photoelectron spectrum is the calculation of an electron binding energy for each peak from the kinetic energy corresponding to its position. For a gas, if changes in the vibrational and rotational energy of the molecules during photoemission are small, the binding energy, E_b, is given by

$$E_b^{\,v} = h\nu - E_{kin} \qquad (1)$$

where $h\nu$ is the energy of the x-ray photons and E_{kin} is the measured kinetic energy of the photoelectron peak. The superscript v in $E_b^{\,v}$ indicates that the reference for zero energy in a gas experiment is an electron at rest in the vacuum.

For solids, the existence of the contact potential, ϕ_c, between the sample and the spectrometer suggests the adoption of a different energy reference. Since the sample and the spectrometer are electrically connected, at equilibrium their Fermi levels are equal. As shown in Figure 5 (9), the kinetic energy of an electron leaving the sample (E'_{kin}) is adjusted by the contact potential so that kinetic energy is measured with respect to the vacuum level of the spectrometer. A binding energy may be calculated from E_{kin} by Equation (2)

$$E_b^{\,f} = h\nu - E_{kin} - \phi_{sp} \qquad (2)$$

where ϕ_{sp} is the work function of the spectrometer and is usually assumed to be constant from experiment to experiment. The superscript f indicates

that the zero of energy is taken for an electron at rest at the Fermi level. Equation (3) relates E_b^f to E_b^v if ϕ_s is taken to be the work function of the sample.

$$E_b^v = E_b^f + \phi_s \tag{3}$$

Before the binding energy corresponding to a particular peak may be taken as indicative of the chemistry of the atom generating the electron, a few additional considerations, particularly for experiments on solids, must be made. When experiments are carried out on semi-conductors or insulators, the sample may become charged due to the depletion of electrons in the sample by the photoelectric effect. This charging effect is common in samples encountered in catalytic experiments but has not been a serious problem in most cases. In some experiments, the carbon (1s) line from pump oil or other contaminants can be used for calibration. A line from any chemically inactive component of a sample can be used as a standard for determining relative chemical shifts. One can also check for charging by changing the x-ray flux impinging on the sample and, therefore, changing the photoelectron current (10). In any case, charging affects all electron levels equally and is sensitive to factors, such as temperature and hydration, which affect the conductivity of a sample.

Also in semiconductors and insulators, surface states can produce a surface potential which is propagated into the solid. The depth of the affected layer can be as much as 10,000 Å and depends roughly on the dielectric constant of the material. In such a case, the Fermi level remains constant, but all electron energy levels are bent in the affected region. Since the analysis depth is ca. 100 Å in solids, such level

bending could appear as a shift or broadening of the photoelectron lines. Little information on this effect is available so far, but such shifts would be a strong function of surface conditions.

Radiation damage during an experiment is another possibility which can lead to erroneous results. In the Berkeley XPS apparatus, the total electron current leaving the sample is about 10^{10} electron/sec. In short experiments, therefore, chemical alterations of the sample due to damage from the photoelectrons is unlikely. In longer experiments, damage is possible in cases where chemical changes caused by the electrons are irreversible or long-lived. Chemical alteration of the sample due to the high x-ray flux can also occur and has been observed in photosensitive samples such as certain alkali halides. In either of these cases, it is often possible to detect radiation damage by the time dependence of the spectrum and/or by comparison of the physical appearance of the sample before and after an experiment. For problems in catalysis, the question of radiation damage is likely to be most important in adsorption studies, where electron or photon induced desorption can take place.

In addition to the photoelectron lines already discussed, other lines can occur in a photoelectron spectrum, and these must be carefully identified to avoid confusion in the interpretation of results. First of these are the Auger lines already discussed. Although Auger lines are the subject of many studies, they are less desirable than photoelectron lines in this context because they are usually broader than photoelectron lines

and are less simply related theoretically to the charge distribution in the sample. Auger lines are easily identified in a spectrum by comparing it to a spectrum of the same sample taken with a different anode and, therefore, a different x-ray energy. The photoelectron lines shift with x-ray energy, but the Auger lines do not.

A second source of additional lines in spectra from solids is discrete energy loss (DEL) processes. These include interband transitions, excitons and plasmons. Peaks of this origin have so far not been carefully investigated by XPS although peaks on the left, or lower kinetic energy side, of a main peak can sometimes be identified as loss peaks (3). In most cases the probability for DEL processes is not a strong function of electron kinetic energy, and neighboring lines should show similar loss structure on the low kinetic energy side. Plasmon lines, possible in metals and semiconductors, may be of particular interest since surface plasmon losses at energies depending on the bulk plasmon frequency and dielectric constant of the surface layer also occur (11). If both surface and bulk plasmon peaks were present on photoelectron lines of different kinetic energy, the relative intensities of the surface to bulk plasmon peaks might reflect differences in the mean escape depth of the photoelectrons studied (12).

Another source of additional lines is the x-ray spectrum itself.

In most spectrometers now in use, little effort is made to filter the exciting x-rays. The spectra from commonly used anodes are simple, however, and all additional lines are well characterized and easily identified [1,3]. When computer fitting is used for spectrum analysis, it is usually advantageous to include even the low intensity x-ray satellite lines in the fit.

The limitations of the measurement of chemical properties by XPS are strongly dependent on the spectral linewidth. First of the three contributions to the linewidth is the width of the exciting x-ray line. The narrowest width obtainable directly from a conveniently usable anode is ca. 0.8eV from the $K\alpha_{1,2}$ x-rays of Mg. The somewhat more energetic $K\alpha_{1,2}$ x-rays of Al, with a slightly larger linewidth, are also often used. The second contribution to the width is the width of the electron level being studied and can range from less then one tenth to several eV. Finally, spectrometer broadening contributes to the width. In a given experiment, the resolution, $\Delta E/E$, of the electron analyzer. is fixed, and the absolute spectrometer broadening, ΔE, is a function of electron kinetic energy. The lowest energy x-ray source, therefore, gives the smallest spectrometer broadening, and for a given x-ray source, electron lines corresponding to higher binding energy have a somewhat lower spectrometer contribution to the width. In the high precision machines being used in XPS, $\Delta E/E$ is adjustable. Instrumental broadening is usually tuned to 0.05 - 0.01% of the electron kinetic energy and is, therefore, of the order of a few tenths of an eV.

Observed total linewidths, then, are of the order of 1 eV or more.

Chemical shifts, which vary from 0 - 10 eV, are often of the same order of magnitude as the linewidth. Extraction of accurate shift values from spectra in these cases is difficult, and it is desirable in many cases to perform a computer resolution of spectra. Such a task is not simple, however, because of the difficulty in estimating the effect of inelastic losses on the lineshape. Two approaches to the fitting problem have been pursued in recent work at Berkeley. The first (3) is an empirical technique in which a response function derived from the characteristics of a sharp single photoelectron peak is applied to the resolution of more complex peaks of only slightly different kinetic energy. The second method [13] approximates the lineshape by a Gaussian or Lorentzian peak with a flat or exponential tail on the low kinetic energy side to account for energy loss. This arbitrary lineshape for each peak in the region of interest is optimized by least-squares analysis (13). Even with computer fitting, however, the resolution of small splittings is difficult. This fact is undoubtedly appreciated by those who work with Gaussian lineshapes. A splitting of two standard deviations (~ 0.9 times the full width at half maximum) between Gaussian lines of equal height and width produces a broadened peak with only one maximum.

C. Extraction of Chemical Information from X-Ray Photoelectron Spectra

A simple classical model (9,1) provides a qualitative understanding of the relationship between XPS chemical shifts and actual charges on atoms. In the model, an ion with charge q is approximated by a conducting sphere of radius r, corresponding to the radial maximum of the valence electron orbitals. The ion with charge q+1 is formed by removal of an electron from the surface of the sphere to infinity. Upon increasing the charge on the ion, the change in potential energy of an electron inside the sphere is given by $-e^2/r$. Thus, the model predicts that the binding energy of all the electrons in an atom will be shifted by the same amount and that the magnitude of the shifts should be of the order of e^2/r or ca. 10eV per unit change in the charge on the atom. Similar predictions result if a calculation of the change in potential of inner shell electrons due to a change in the number of valence electrons is made by the unrestricted Hartree-Fock method (9). Deviations from Koopman's Theorem, important in interpretation of these calculations, are discussed in [1] and [3].

In molecules and solids, a valence electron is removed not to infinity by a change in the oxidation state, but to some distance roughly equal to the nearest neighbor separation. The expression for the change in potential in the atom must then be modified to read $-e^2/r + e^2/R$ where R is approximately the nearest neighbor distance. Applications of a variation of the charged-shell

model to europium compounds are given by Fadley et al. (9). Europium is particularly interesting because oxidation from Eu^{2+} to Eu^{3+} corresponds closely to the actual removal of one electron from the 4f orbital. Since oxidation of Eu^{2+} corresponds to nearly a unit change in the actual ionic charge, the classical model qualitatively predicts the large shifts which are observed.

An alternative model for the calculation of shifts in solids divides the photoelectric process into three steps (9). Level i of ion A with charge z is assumed to be the electron level of interest. In step one, A is removed from the solid. In step 2, an electron is ejected from level i of A, producing an ion with charge z + 1. Then A is re-introduced into the solid. The net result is the process of interest; the production of a photoelectron ejected from the solid. The cycle leads to Equation (4), for the chemical shift of A with charge z in solid X with respect to A with charge z' in solid Y.

$$\Delta E_b^f = \Delta E_b^v\ (A,i,z-z') + \Delta(E_1 + E_2) + \Delta\phi_C \qquad (4)$$

where

ΔE_b^f = Fermi-reference binding energy shift.

$\Delta E_b^v\ (A,i,z-z')$ = shift in vacuum-referenced binding energy for an electron in the i-th level of free-ion A with charge z vs. z'.

$\Delta(E_1 + E_2)$ = difference, between X and Y, in the sum of the

energies for extracting atom A with charge q from the solid and that for replacing A with charge q + 1 into the solid.

$\Delta\phi_C$ = difference in contact potential of X and Y with respect to the spectrometer.

As shown by Fadley et al., [9] neglect of $\Delta\phi_C$ and polarization effects and consideration of only point charge Coulombic forces between ions lead to Equation (5),

$$\Delta E_b^f = \Delta E_b^v (A,i,z-z') + \Delta E_m(+1) \qquad (5)$$

where $E_m(q) = e^2 q \sum_k q_k/r_{Ak}$; r_{Ak} is the distance between the ion of interest, A, and the other ions, k, in the solid; and $\sum_k$ is a sum over the entire lattice.

The ΔE_b^v (A, i, z-z') term, or free-ion term, in Equation (5) is equivalent to the e^2/r term in the classical model. The Hartree-Fock calculations of Fadley et al. indicate that the size of this term increases toward the upper right hand corner of the periodic table. The $\Delta E_m(+1)$ term indicates the necessity of considering the lattice potential at the site of the atom emitting the photoelectron and is equivalent to the e^2/R term in the classical or shell model. The contact potential difference, $\Delta\phi_C$, is probably $\leq$ leV, but its neglect is primarily due to the lack of sufficient work function data and represents a current limitation in the interpretation of XPS shifts. Correlations, such as that in Figure 1, show that a roughly linear relationship exists between calculated charge on an ion and the measured binding energy of its electrons.

The existence of two lines in Figure 1, however, may be a result of the neglect of the second and third terms in Equation (4).

An alternate approach to the analysis of chemical shifts uses a cycle similar to that discussed above but relates the various energies to thermodynamic quantities [14]. Application of this scheme is also restricted by several assumptions, but good correlations of shifts in certain classes of compounds have been found and the use of shifts for prediction of some thermodynamic quantities has been demonstrated (14).

Although the relationship between chemical shifts and atomic charge has received the most attention, other effects of chemical interest have also been studied by x-ray photoelectron spectroscopy. One such effect is the splitting of the $p_{3/2}$ levels in heavy atoms. Novakov and Hollander [15] report x-ray photoelectron spectra showing splittings of the $5p_{3/2}$ levels of Th metal, U metal and UO_3. The $4f_{5/2}$ and $4f_{7/2}$ lines of the same samples were unsplit. A more recent study by those authors (16) indicates that similar splittings found for the Au $5p_{3/2}$ levels in gold compounds correlate linearly with the Mössbauer quadrupole splittings of the compounds. This result suggests that the $p_{3/2}$ level splittings may be related to the electric field gradient within the atom and that in some cases XPS will provide information about the symmetry of the atomic environment.

Another type of core level splitting, multiplet splitting, arises primarily from the exchange interaction between core electrons and unpaired

valence electrons [3] . Such effects have now been observed in paramagnetic gases (17) and in solids (18). In some cases, these splittings may be used to identify spin states of paramagnetic ions [18].

Since studies in catalysis are oriented primarily towards surface phenomena, the electron escape depth in x-ray photoelectron measurements on solids is of great importance. Although thorough quantitative investigations have not yet been undertaken, some pertinent data are summarized in Table 2. The first two entries are the results of an experiment by Palmberg and Rhodin (19) in which low energy electron diffraction and Auger spectroscopy were combined to measure the intensity of Auger electrons as a function of the number of monolayers of silver covering a gold single crystal. The third entry is the result of the experiment by Siegbahn et al., shown in Figure 2. As expected, the escape depth depends on both the atomic number of the material and the kinetic energy of the electrons. In general, fast electrons from low Z materials probably sample the bulk, while slow electrons from high Z materials should be expected to show a strong surface influence. In principle, one can differentiate bulk from surface effects by measuring spectra of both high and low kinetic energy electrons from the same sample. Differences in the two spectra could then be used to deduce surface chemistry.

The electron escape depth is also an important factor in the interpretation of the chemical composition of heterogeneous samples from peak areas. With careful calibration and a study of lines at several

Table 2

Mean Escape Depth of Electrons in Solids

Solid	Electron Kinetic Energy	Mean Escape Depth	Ref.
Ag	72 eV	4 Å	19
Ag	362 eV	8 Å	19
Iodostearic Acid	860 eV	< 100 Å	1

kinetic energies, one should be able to use the composition corresponding to various electron escape depths to differentiate between a solid solution versus surface segregation of a particular species. Because of the relatively low escape depth for electrons in many experiments, a study of several electron lines (perhaps using a Cu or Cr as well as Mg or Al anode) may be needed before a reliable assignment of the chemical composition of the bulk or surface layer can be made.

Even if a solid sample is homogeneous all the way to the surface, the atoms at the surface experience a different crystal potential than those in the bulk [9]. Thus, the $E_m(+1)$ term in Equation (5) is altered at the surface (and approaching the surface) and can lead to a chemical shift between surface and bulk atoms. If the $E_m(+1)$ term for a particular solid is known, $E_m(+1)$ for a surface atom ($E_{m,s}(+1)$) may be calculated (20) by Equation (6),

$$E_{m,s}(+1) = [E_m(+1) - E_s(+1)]/2 + E'_s(+1). \qquad (6)$$

The surface is defined by a plane passing through the crystal. The term $E_s(+1) = e^2 \Sigma_i q_i/r_{Ai}$, where i is summed over the atoms in the plane. The term $[E_m(+1) - E_s(+1)]/2$, then, represents the potential due to a semi-infinite crystal, up to, but not including, the surface plane. The term $E'_s(+1) = e^2 \Sigma_j q_j/r_{Aj}$, where j is summed over the correctly terminating surface plane of interest. The surface plane may include defects or adatoms but must terminate the crystal to preserve

charge neutrality. For the NaCl structure $E_m(+1) = \pm \frac{e^2\alpha}{R_o}$, where R_o is the cation-anion distance and α is the reduced Madelung constant. For an infinite crystal, $\alpha = 1.75$. For atoms at the (100) surface of a semi-infinite crystal, $\alpha = 1.68$, assuming that the surface is terminated with a complete plane of atoms. For a surface atom adjacent to an NaCl vacancy, α can be as low as 1.18. Thus, $E_m(+1)$ is decreased in magnitude by only about 4% at a perfect surface, but by as much as 30%, or about 4eV, adjacent to a surface defect. If the charges on the surface atoms are similar to those on atoms in the bulk, then surface shifts of the order of 1eV and higher should be expected. Experimentally, such effects would most often appear as a broadening of a photoelectron line, since atomic layers near the surface are also partially affected. In many cases linewidths of photoelectron lines from solids are less than 2.5eV, and in no case has an extreme broadening due to surface shifts been reported. Little work has been done so far, however, on the determination of natural linewidths or on clean surfaces, to which the above estimates apply.

Summarizing, we find that the measurement and assignment of x-ray photoelectron peaks are direct. The interpretation of data is easiest for gases, but the spurious effects encountered in some measurements on solids can often be corrected for or at least recognized. The Fermi level reference for solids complicates a detailed interpretation of chemical shifts, but useful correlations of shifts with ionic charges or thermochemical data are possible. Under most conditions, x-ray photoelectron

spectroscopy is only a semi-surface technique, but several aspects of the measurements relate directly to surfaces.

III. EXPERIMENTAL EQUIPMENT

This section describes the functional components of an x-ray photoelectron spectrometer and summarizes, based on our experience, several operating characteristics desirable for research in catalysis. The reader is referred to (1, 21, 22) for the details of spectrometer design. Figure 6 is a schematic diagram of the Berkeley iron-free spectrometer. The main components are the x-ray source, the sample chamber, the electron analyzer and the electron detector.

In the x-ray tube, a high voltage between the cathode and anode causes electrons emitted from the heated tungsten cathode to be accelerated and strike the anode to produce the desired x-rays. Typical anode materials are Mg, Al, Cr and Cu. Consideration of linewidth and energy of the x-rays dictates anode choice. A multiple position anode allowing quick change from one anode material to another is convenient. The x-rays pass through a window, usually thin Be or Al, to the sample. The purpose of the window is to prevent electrons in the tube from reaching the electron analyzer. Geometric restrictions and the need for iron-free construction in magnetic spectrometers often require custom construction of x-ray tubes. It is advantageous to have an indirect electron path from cathode to anode so that tungsten from the cathode does not condense on the anode or the window. Also, an isolated

vacuum system for the tube is desirable, in spite of the difficulties caused by the presence of the fragile Be or Al window. Otherwise, gases introduced into the sample chamber during an experiment may cause rapid deterioration of the tube.

Although monochromatization for narrowing the x-ray linewidth would often be desirable, the associated sacrifice in intensity must be compensated by means of higher electron flux striking the anode [1]. As mentioned in the Fundamentals section, excitation of photo electrons by ultraviolet radiation and production of Auger electrons by electron bombardment are also of interest in electron spectroscopy. The availability of such sources would increase the versatility of a photoelectron spectrometer.

The arrangement of the radiation source, sample, and the analyzer must be such that photons or electrons from the radiation source can strike the sample, and electrons emitted from the sample can pass through the defining slit into the electron analyzer. In light of experiments in Auger spectroscopy [23], an enhancement of the influence of surfaces on the x-ray photoelectron spectra of solids might be achieved by working at low angles between the plane of the surface and the electron path to the analyzer. No such experiments have yet been reported in photoelectron studies of solids.

In order to minimize scattering of electrons during analysis, the pressure in the analyzing chamber should be about 10^{-5} torr or lower.

Any gases in the sample chamber must, therefore, be differentially pumped across the defining slit. In some experiments, introduction of the gaseous sample in a molecular beam may facilitate pumping. With differential pumping, experiments on gases can be done easily [1]. Low vapor pressure liquids may also be studied if the spectrometer geometry permits a horizontal sample surface. Otherwise liquids can be frozen or studied as continuous, flowing thin films.

An important consideration for XPS studies in catalysis, as well as other fields, is the vacuum required in the sample chamber. For low-area samples, simple kinetic theory calculations show that pressures lower than about 10^{-9}torr are needed for clean surface studies. However, Eischens has argued that pressures from 10^{-6} to 10^{-4}torr are adequate for infrared studies of catalyst samples with high adsorptive capacity(24). This view is supported by much infrared evidence that easily oxidized, adsorbed species such as carbon monoxide and hydrogen are stable for many hours on supported metal catalysts in vacuum systems which cannot be operated at pressures lower than 10^{-6}torr. In infrared experiments, all of the catalyst wafer is examined by the radiation. In a photoelectron experiment, however, the advantage of the self-gettering action of the wafer may be minimized because only the outer surface layers are examined, and these exposed layers may become contaminated sooner than the inner portions of a sample. We expect, therefore, that reproducibility and clear interpretation of results from solid samples with reactive surfaces will require better vacuum conditions in the

sample chamber than are needed for infrared studies. In many cases, ultrahigh vacuum may be needed. In addition, great care must be taken to limit contamination from oil pumps. In any case, it is desirable that the sample chamber be designed so that pretreatment of samples may be carried out in a controlled environment.

After electrons leave the sample chamber, their kinetic energy must be carefully measured in the electron analyzer. The resolution of the analyzer should be of the order of a few parts in 10^4 in order that the spectrometer broadening for high kinetic energy electrons be of the order of a few tenths of an eV. The second important characteristic of the analyzer is high sensitivity in order to minimize the counting times required for the collection of data. In general, double focusing devices (25) are employed to achieve both of the above requirements. In some cases, retardation of electrons is used to improve resolution. Since higher resolution is usually accompanied by a sacrifice of sensitivity, it is desirable that a spectrometer have tunable resolution.

Both magnetic and electrostatic double focusing analyzers have been used [1,21]. Magnetic devices now in use have optical paths 30-50 cm in radius, and focus electrons in the region between sets of solenoidal deflection coils. This configuration restricts the working space around the sample chamber. A new coil configuration reported by Fadley, Miner and Hollander (22) uses the field external to the coils and allows much greater accessibility to the source.

The magnetic, double focusing analyzer has the advantages that electrostatic fine tuning is possible and the sample and analysis chambers are readily adaptable to ultrahigh vacuum. The focal plane characteristics of this design and some electrostatic designs will become increasingly important with the advent of small multichannel electron multipliers. The large enhancement in counting efficiency provided by such detectors is further discussed in (22).

The disadvantage of the magnetic analyzer is that elaborate methods are required for shielding the analyzer from external fields. Typically, the spectrometer is placed in the center of a large Helmholtz coil arrangement and care must be exercised to exclude high-permeability materials from the immediate vicinity. Other types of shielding may also be possible, but none has yet been developed.

A principle advantage of the several electrostatic analyzers that have been developed is that shielding may be placed close to the analyzer without distorting the deflecting field, and a controlled environment is not needed. This type of device is, therefore, better suited than the magnetic one for a standard laboratory. In general, the performances of existing electrostatic and magnet analyzers are comparable, although particular spectrometers have strong and weak features. In some electrostatic spectrometers, large slits are used to enhance sensitivity. Differential pumping of gases in such devices may be difficult. In electrostatic analyzers, the deflecting plates must be within the walls of the vacuum chamber. Dimensional instability as a result of bake-out may complicate ultrahigh vacuum studies in such spectrometers.

In an experiment, the analyzer is set to focus electrons of a certain kinetic energy on the detector. Various kinetic energies are scanned by changes in the analyzer field settings or changes in the retarding potential. The detector is usually a windowless electron multiplier which produces a pulse for each electron reaching the detector. The pulses are then counted and recorded. In an instrument having a focal plane, each row of electron multipliers in a multichannel unit counts electrons of a slightly different energy. Thus several data points can be taken simultaneously. Scanning of the analyzer fields may be continuous or point by point. In either case, a small programable computer provides the greatest versatility for efficient collection of data.

IV. EXPERIMENTAL RESULTS AND DISCUSSION

The data reported here were taken on the Berkeley 50 cm iron-free spectrometer (Figure 6). Two types of three-position holders for solid samples (26) were used. The room temperature holder had no provision for differential pumping. Powdered samples were usually sprinkled on double-sided, conducting tape. In some cases pressed wafers, 13 mm in diameter and about 1 mm thick, were taped to the holder. In the heated sample holder the defining slit was mounted on a stainless steel chamber enclosing the samples. The x-rays were admitted

through a Be window. Metal foil or pressed wafer samples were held at the edges on a boron nitride heater by a stainless steel cover plate. In situ treatment in hydrogen was accomplished by admitting hydrogen to the sample enclosure through a stainless steel tube directed toward the sample surface. The hydrogen pressure around the sample was approximately 10^{-2}torr or less. The detector chamber, sample chamber, x-ray tube, and analysis chamber were pumped by a silicone oil diffusion pump, backed by a mechanical pump. The inlet to the diffusion pump was in the analysis chamber. The base pressure, measured just above the liquid nitrogen trap above the diffusion pump, was usually less than 10^{-5}torr. The pressure in the sample region was not measured, but could have been 10^{-4}torr in some experiments. Although the diffusion pump was well trapped, a large lucite viewing port, rubber o-rings, and a poorly trapped mechanical roughing pump for the sample chamber contributed carbon containing molecules to the background gas. The vacuum conditions were less than ideal, but the data shown in Figure 3 indicate that relatively clean surface layers could be maintained at high temperature in hydrogen.

In figures to follow, data are reported as plots of electrons counted versus the current in the deflecting coils of the spectrometer. Except where indicated, the data presented have been corrected for sample charging by adjusting energies so that the kinetic energy of the C (1s) line from carbon contamination on the sample was equal to the energy of the C (1s) line from a metal foil placed in one of the two remaining sample positions. In the Cu/MgO experiments the Mg (2p) line was used to make

a relative charging adjustment. Because of the reactivity of the surfaces studied in experiments on catalysts, charging corrections using the carbon line from carbon contamination may not be reliable. Splittings in a single sample and shifts between similar samples should be unaffected by charging. Comparisons of line positions from dissimilar samples, however, are highly susceptible to errors in the charging correction.

In this work, charging corrections as high as 3-5eV have been required. Because of the magnitude and uncertainty of this correction, we have not reported absolute binding energies. The kinetic energy corresponding to a particular peak may be obtained from the table of kinetic energy vs. magnetic rigidity ($\beta\rho$) in Appendix 5 of reference (1), using a value of $\beta\rho$ calculated from Equation (7),

$$\beta\rho = C \cdot I, \tag{7}$$

where I is the current value, in amps, of the peak position and C is the spectrometer calibration constant. It has been assumed that the binding energy of the C (1s) electron in a hydrocarbon adsorbed on a metal is the same as that for graphite. The data in (10) then yield $C = 78.706 \frac{\text{Gcm.}}{\text{amp}}$ for most of the spectra reported here. Except where indicated, all spectra were taken with an Mg anode so that $h\nu = 1253.6$eV. The work function of the spectrometer, ϕ_{sp} is taken to be 4 eV [2]. Splittings of lines may be calculated by Equation (8),

$$\Delta E \cong 1.09\ (\Delta I)\ \bar{I} \tag{8}$$

where

ΔE = splitting in eV

ΔI = splitting in ma.

$\bar{I}$ = the average of the currents of the two peaks, in amps.

Experiments were carried out in three general areas: adsorption, supported metals and crystalline oxides.

A. Adsorption

As mentioned in the Introduction, large shifts have been measured for several carbon and nitrogen containing molecules. Since some of these molecules are common participants in catalytic reactions, studies of carbon and nitrogen containing molecules adsorbed on catalyst surfaces seem to be an interesting and important application of x-ray photoelectron spectroscopy. The data of Siegbahn et al., represented in Figure 2, show that a spectrum of the I($3d_{5/2}$) line from a double layer of iodostearic acid can be collected in a few minutes. In order to estimate the counting times required to see a monolayer of adsorbed carbon containing molecules, one must know the relative cross-section for the photoelectric effect in the C (1s) levels as compared to the I ($3d_{5/2}$) level. This information is readily obtained from the data for gas phase methyl iodide shown in Figure 7. The relative areas under the curves indicate that for magnesium x-rays the I ($3d_{5/2}$) cross-section is 13 times that for C (1s), while the same ratio is 17 for aluminum x-rays. Although the gas pressures were not identical for the Mg and Al anode experiments,

the data indicate that approximately 3 minutes per point should be the required counting time for observation of a carbon monolayer on a metal foil in a spectrometer with the same overall spectrometer sensitivity as that used to obtain Figure 2.

Since CO is strongly held to Pt and is oxidized to CO_2 and desorbed only slowly even in the presence of small amounts of O_2 (27), we chose to attempt observation of CO on platinum. For prereduced Pt foil and 5% Pt on SiO_2 (56% dispersed), measurable carbon and oxygen lines were observed in counting times of ~0.3 min/point, but they were identical to lines present before CO adsorption. Since the ratio of spectrometer sensitivities in these experiments and those carried out on iodostearic acid is unknown, it is not possible to accurately estimate the amount of carbon present on the Pt samples. Clearly, however, the carbon and oxygen backgrounds were high enough to mask CO adsorption effects. Although the experiment was a negative one, it represents a limit of the vacuum conditions in the particular spectrometer and not of the technique.

Studies of nitrogen containing molecules adsorbed on high-surface area materials are experimentally more favorable because of the increased

number of adsorbed atoms and a negligible nitrogen background. A study of nitrogen containing Y zeolite is shown in Figure 8. Spectrum8(a) is for an 85% exchanged NH_4Y zeolite wafer. Because of the high exchange capacity of the zeolite, spectrum8(a) represents an approach to the upper limit in intensity to be expected from an adsorption experiment of the type discussed here. The total counting time required for that spectrum was over 7 hours, but, with fewer points, could have been reduced to about four hours. The desirability of high spectrometer sensitivity is thus quite clear. The position of the nitrogen (1s) line in 8(a) corresponds to a binding energy of 402 eV, in good agreement with the value for NH_4^+ in NH_4NO_3 as shown in Figure 1.

Spectrum8(b) was taken after the wafer giving spectrum8(a) was heated to 150°C for ~10 hours in vacuo. Spectrum8(b) shows, as expected, that more than half of the nitrogen had been desorbed by the heat treatment. The increase in the linewidth may indicate the presence of two or more chemical states of nitrogen, but the counting statistics were not sufficient to permit resolution of the peak components. In other experiments, a wafer of silica-alumina was evacuated at room temperature, exposed to 1 atm of NH_3 and then transferred through the air to the spectrometer. Also, a wafer of NH_4-Y zeolite was deammonated at 10^{-3} torr at 550°C, exposed to 1 atm of NH_3 at room temperature and transferred to the spectrometer. The N (1s) spectra of both of these wafers were similar to8(a) but lower in intensity. Both spectra showed a broadening and decrease in intensity after evacuation at 150°C.

Spectrum (c) of Figure 8 was taken after the wafer giving8(b) was heated in situ in a low pressure of H_2 for 4 hours at 350°C and 1 hour at 450°C, then cooled to 120°C, and exposed to pyridine at a pressure of approximately 5 torr. The hydrogen was employed during heating in order to try to keep the sample surface free of the hydrocarbons present in the spectrometer. Spectrum 8(c) is a broad doublet with a splitting of 3.4eV. A similar experiment on an NH_4Y wafer heated to 450°C and cooled to 150°C gave a broad N (1s) peak at a current of 1.2486 amp. Thus, it is assumed that the left peak in 8(c) is due to residual nitrogen from NH_4Y and right peak is due to adsorbed pyridine. Estimates of peak areas indicate that, based on the above assignment of peaks, approximately 30% of the original nitrogen was left in 8(c) and the adsorbed pyridine corresponded to approximately 15% of the original nitrogen.

The shift in the residual nitrogen line in8(c) was supported by a later experiment in which NH_3 adsorbed at 120°C on an Eu^{3+} exchanged mordenite wafer (dehydrated 10 hours at 450°C) gave a broad N (1s) line at 1.2492 amps. The effect of dehydration on the nitrogen in the zeolite could involve removal of H_2O from the coordination sphere of NH_4^+ ions not in the hexagonal prisms. At 450°C, some dehydroxylation of the zeolite surface accompanies deammonation, and the resulting Lewis acid sites could adsorb NH_3. Removal of water from the zeolite pores can also change the lattice potential at the nitrogen atom site.

Although it is not possible to make chemical inferences about adsorbed pyridine from the results of spectrum 8(c) alone, the

spectrum shows that the adsorption can be observed. The shift between the NH_4^+ line in8(a) and the pyridine line in8(c) is similar in magnitude and sign to the shift between NH_4^+ in NH_4NO_3 and pure pyridine, as shown in Figure 1.

Thus, different nitrogen-containing molecules adsorbed on high surface area materials can be observed in the x-ray photoelectron spectrum and chemical changes in those molecules recorded. More detailed studies of the actual chemical states of the molecules involved would be aided by higher spectrometer sensitivity and a better control of the environment of the samples.

B. Supported Metals

Dispersion of active metals on supports is a technique widely used in catalysis to improve the catalytic efficiency per metal atom. X-Ray photoelectron spectroscopy offers the possibility of studying changes of both the oxidation state of various atoms and the chemical composition of surface layers during the preparation of such materials. Interactions of activated catalysts with adsorbed or reacting gases are also amenable to study if chemical changes in the surface layer are significant at gas pressures below 10^{-1} torr.

In an attempt to study the chemical states of surface atoms, a series of experiments on supported and unsupported Pt was undertaken. The Pt $(4f_{5/2})$ and $(4f_{7/2})$ lines from several samples are shown in Figure 9. Spectra 9(a), 9(d) and 9(e) have been adjusted for charging but spectra

9(b) and9(c) have not. A comparison of spectrum9(d) with9(a) shows a shift of 3.8 eV for Pt atoms in a foil versus Pt ions in PtO_2. As the energy dependence of the photoelectric cross section per electron is essentially the same for the $4f_{5/2}$ and $4f_{7/2}$ levels, the theoretical ratio of the area of the $4f_{7/2}$ (right) peak to that of the $4f_{5/2}$ (left) peak is 1.33, as determined by the degeneracies of the levels. Computer fitting with 2 Gaussian peaks with flat tails gave estimates of 1.4 and 1.1 for the $4f_{7/2}/4f_{5/2}$ area ratios of9(a) and9(d) respectively. An x-ray diffraction pattern of the PtO_2 powder showed the presence of a small amount of platinum metal. This observation is in agreement with the high value of the peak ratio in spectrum9(a) since the low intensity Pt metal peaks contribute to the area of the $4f_{7/2}$ line of PtO_2.

As mentioned in the Fundamentals section, the Gaussian peak with a flat tail is only an approximation of the line shape. The reliability of the calculated area ratios is, therefore, uncertain. The data in Table 2 suggest, however, that electrons have a low mean escape depth through heavy metals. In addition to their results for Ag deposition on Au, Palmberg and Rhodin (19) estimated a mean escape depth of 3 to 4 monolayers for 950 eV Cu Auger electrons through gold deposited on copper. On the basis of these data, a small influence of the surface layer could be present in the Pt foil spectrum9(d). Since the foil had been exposed to the atmosphere, it was probably covered with a layer of oxide during the experiment. Peaks from the oxidized Pt atoms would fall under the left ($4f_{5/2}$) peak in9(d) and could, therefore, account

for the low area ratio. This hypothesis is supported by the fact that a Pt black sample, having a higher surface to volume ratio than the foil, gave an area ratio of 1.0. A definitive test of surface effects will require accurate control of surface conditions, however.

Spectra (b) and (c) in Figure 9 are for 5% Pt on SiO_2, prepared by impregnation of SiO_2 with chloroplatinic acid and prereduction before transfer to the spectrometer. The platinum was found to be 56% dispersed (i.e., 56% of all the Pt atoms were on the surface) by CO chemisorption measurements (28). Since no charging correction was made, shifts between spectra cannot be evaluated. The shift to the right with increased temperature, however, is similar to that attributed to a change in the amount of charging in Cu/MgO and zeolite samples. The relative intensities of the $4f_{5/2}$ and $4f_{7/2}$ lines in spectra 9(b) and 9(c) clearly indicate the presence of oxidized Pt. Similar peak ratios were found for the Pt/SiO_2 sample at room temperature. One must recall that the term "in H_2" means in a low pressure flow of H_2. Apparently, in the configuration used to obtain the results shown in Figure 9, the H_2 pressure at the sample surface was not high enough to maintain significant reduction. An improved experimental configuration allowed partial reduction of oxidized Pt as shown in Figure 10, for a 1% Pt on graphon sample (29). The dispersion of this sample was approximately 20%. Spectrum 10(c) is for a prereduced sample, exposed to air before the XPS experiment. The area ratio of this spectrum was 1.1. A wafer of the same material was heated to $300^{o}C$ in flowing oxygen for 1 hour before transfer to the spectrometer to yield 10(a).

The breadth of the $4f_{5/2}$ (left) line of that spectrum may indicate the presence of Pt in more than one oxidation state. Partial reduction of the most highly oxidized Pt by H_2 treatment in situ is shown in 10(b) by the narrowing of the $4f_{5/2}$ line. This spectrum is similar to (b) and (c) in Figure 9. Although it seems clear from the spectra for supported Pt in both Figures 9 and 10 that the relative intensity of the $4f_{5/2}$ and $4f_{7/2}$ lines indicate the presence of oxidized Pt, a quantitative assignment of the oxidized species was not possible. Spectra (b) and (c) in Figure 9 cannot be accounted for by the assumption that the increased intensity of the left peak was due to 56% of the Pt being present as PtO. At this time, therefore, the spectra can be taken as only a qualitative indication of an effect of dispersion on the oxidizability of platinum.

A second study of supported metal was done on a 5% Cu on MgO sample prepared by impregnation of MgO with a solution of cupric acetate in ethanol (30). The carbon (1s) lines from MgO and MgO impregnated with cupric acetate are shown in Figure 11. The large right peak is due to adsorbed carbon-containing material from the background gas and is assumed to represent adsorbed hydrocarbons. The left peak in spectrum 11(b) is shifted 3.9 eV from the hydrocarbon peak. The splitting of the C (1s) line in sodium acetate is approximately 3.6 eV (1, p.79). Thus, assignment of the left peak in spectrum 11(b) to acetate ion on the MgO surface seems reasonable. The broadening of that peak may indicate some chemical interaction of the acetate ions with the MgO

surface. After heating the sample giving spectrum 11(b) to 500°C in H_2, the left peak was not observed in the C(1s) spectrum.

Spectrum (a) of Figure 11 shows a weak peak 4.8 eV from the carbon background peak. This large shift to higher binding energy indicates the presence of carbon atoms more highly oxidized than those in the acetate. On this basis, the peak is assumed to be due to $CO_3^=$ or HCO_3^-, formed on the MgO surface by adsorption of CO_2 from the air. The O(1s) line from MgO at room temperature in vacuo had a shoulder on the high kinetic energy side, indicating the presence of more than one kind of oxygen on the MgO surface. Under these conditions, OH^- and H_2O, in addition to $CO_3^=$ and HCO_3^- are likely surface species (31).

The copper on MgO was studied by taking both Cu (3p) and Cu ($2p_{3/2}$) spectra. The Cu (3p) region, however, was obscured by a strong peak from the MgO support. Subsequent work on MgO has shown this peak to be a magnesium KLL Auger line. Since magnesium x-rays do not have sufficient energy to eject a 1s electron from Mg, the Auger peak was presumably caused by Bremstrahlung from the x-ray tube which was operated at 12 kilovolts and 20 milliamps.

The Cu ($2p_{3/2}$) spectra are shown in Figure 12. Spectrum 12(a) was produced by a sample calcined at 1000°C in air in an attempt to form a Cu/MgO solid solution. Spectrum 12 (b) is for the impregnated sample, dried by evaporation and not heated. Both peaks are broadened and a splitting into at least two components is evident in spectrum

12(b). Because of the oxidizing conditions used in the preparation of the sample giving 12(a), the broad line is taken to indicate Cu^{2+} on and/or in the surface layer of MgO. The doublet in 12(b) can be accounted for by some cupric acetate and some Cu which is bonded to the MgO surface. A small multiplet splitting [18] or splitting of the type found for heavy atoms (15) cannot be ruled out at this time, however. The ratio of the area (counts/sec x amps) under the Cu ($2p_{3/2}$) line to that under the Mg (2p) line was 0.4 for spectrum 12(a) and 0.9 for 12(b).

Spectrum (c) in Figure 12 was taken after the Cu acetate/MgO sample giving 12(b) was heated to 500°C in low pressure H_2 in situ. The narrowing of the Cu ($2p_{3/2}$) peak indicates that one Cu species predominated over others in the product produced by the reducing treatment. The shift of the line to lower binding energy suggests that reduction of the Cu^{2+} was accomplished. When the position of the peak in 12(c) is compared to that for Cu foil shown in spectrum 12(e), however, it is clear that all factors have not been accounted for. Spectrum 12(c) appears to show a Cu ($2p_{3/2}$) binding energy lower than that for Cu metal. It is likely that the shift between 12(c) and 12(e) is an artifact caused by an inadequate charging correction. Spectra 12(a)-(d), on the other hand, showed a good internal consistency since the Mg (2p) line in all samples fell close to the same value after the C (1s) charging correction was applied. In Figure 12, a slight adjustment has been made on these spectra to bring the Mg (2s) lines into coincidence. On the basis of the present

data, a meaningful comparison between supported Cu and Cu foil cannot be made, but we take the shift between 12(b) and 12(c) to indicate reduction of Cu^{2+}.

The area ratio of the Cu ($2p_{3/2}$) line to the Mg(2p) line in spectrum 12(c) was 0.3. The loss in the amount of Cu measured by XPS in 12(c) versus 12(b) can be explained by sintering of the Cu-containing particles. Some of the Cu may also have gone into solid solution and/or migrated into the MgO pores. Photoelectrons from the Cu deep in the pores or in the bulk have less chance of escaping from the solid than do photoelectrons from Cu on the outer surface of the MgO particles. A similar loss in Cu intensity was noticed in the Cu (3p) spectrum of the "solid solution" heated to 500°C in H_2.

A Cu/MgO wafer which was prereduced at 500°C in flowing H_2 and then transferred to the spectrometer and heated to 530°C in a low pressure of H_2 gave spectrum 12(d). The reduction of the Cu in this sample appears to be more complete than in 12(c). The data suggest assignment of 12(d) to copper metal and 12(c) to Cu^+, but such an assignment would require further calibration with shifts in known compounds and a more complete understanding of the charging corrections for this system.

A clearer observation of reduction of a supported metal was afforded by a study of 6% nickel on silica-alumina (32). Characteristics of the Ni ($2p_{3/2}$) lines from nickel metal and black NiO [33] are shown in Figure 13. Spectrum 13(d) for NiO has two peaks, split by 6.1 eV. Spectrum 13(c), from Ni foil "off the shelf," has peaks similar to those

in 13(d) and an additional peak to the right. When nickel foil was sanded to expose fresh surface, spectrum 13(b) was obtained. This spectrum shows an enhancement of the right peak in 13(c) and a relatively low intensity of the two left peaks. Spectrum 13(a), for a polished Ni (111) single crystal (34), is similar to 13(b).

Since the Ni foil "off the shelf" was stored in air, the surface layer of the foil is expected to be oxidized. The similarity of the left peaks in 13(c) and the peaks in the NiO spectrum leads to assignment of the left peaks in 13(c) to a surface layer of NiO and the right peak to nickel metal. Sanding the foil is then seen in 13(b) to have removed a considerable amount of the oxide, exposing more Ni metal.

The wide split doublet spectrum for NiO is an unexpected result and requires further examination. The O (1s) line of NiO did not show any splitting or any indication of a second peak at 6.1 eV lower kinetic energy from the main peak. The left peak in 13(d) could, therefore, be characteristic of Ni and not a discrete energy loss characteristic of the NiO. Adsorbed water or oxygen on the NiO could mask a loss peak in the O (1s) spectrum. This possibility cannot be definitely ruled out at this time, but such an interpretation would require the peak from adsorbed oxygen-containing molecules to have been ten times more intense than the oxygen peak from NiO.

A doublet with approximately the same splitting and intensity ratio as shown in 13(d) has also been observed in the Ni ($2p_{\frac{1}{2}}$) and (3s) lines of NiO (35). Since multiplet splittings should be different for s, $p_{\frac{1}{2}}$

and $p_{3/2}$ levels (18), it seems unlikely that the splitting is caused by the unpaired electrons of the Ni^{2+} ion. On the other hand, it is known (33) that black NiO is non-stoichiometric, containing excess oxygen and some Ni^{3+}. The shift of 6.1 eV is large for Ni^{2+} to Ni^{3+} but large shifts in electron binding energies of impurity atoms in a lattice are suggested by the following, crude approximation for Ni^{3+} in NiO. If NiO is assumed to have the NaCl structure and to be 50% ionic, then $E_m(+1) = -12eV$. The shift of 3 eV between Ni metal and the right peak of NiO and the use of Equation (5) yield

$$\Delta E_b^{\,v}(Ni, 2p_{3/2}, 0\text{-}+1) = 15eV. \qquad (9)$$

Assuming that the actual charge on Ni^{3+} in NiO would be +1.5 units in analogy to the +1 charge for Ni^{2+}, $\Delta E_b^{\,v}$ above may be scaled to give

$$\Delta E_b^{\,v}(Ni, 2p_{3/2}, +1\text{-}+1.5) = 7.5eV. \qquad (10)$$

If, following (33), Ni^{3+} is placed in the NiO lattice by substituting 2 Ni^{3+} for 3 Ni^{2+} and leaving an Ni^{2+} vacancy, $E_m(+1)$ for the Ni^{3+} site = -12 to -13.5 eV, depending on the positions of the vacancy and the second Ni^{3+} ion. Then, using Equation (5),

$$\Delta E_b^{\,f}(Ni,\ 2p_{3/2}, \text{"}Ni^{3+}\text{" in NiO - "}Ni^{2+}\text{" in NiO}) = 7.5 \text{ to } 6.0 \text{ eV}. \qquad (11)$$

Because of the uncertainty of the calculation and the relatively

large surface concentration of Ni^{3+} implied, this assignment of the NiO spectrum must be considered tentative. Studies of the more nearly stoichiometric, green NiO and in situ oxidation experiments should provide the information necessary to test the assignment.

Even without assignment of the left peak in the NiO spectrum, (d) in Figure 13 can be taken as a "fingerprint" characteristic of NiO. Such a point of view is useful for the interpretation of the Ni ($2p_{3/2}$) spectra of 6% Ni on silica-alumina shown in Figure 14. Spectrum 14(a) resulted after the $Ni(NO_3)_2$ impregnated support was calcined 2 hours in air at 760°C and a wafer of the material was transferred to the spectrometer. The strong resemblance of this spectrum to the one characteristic of NiO is taken to indicate that Ni is present on the catalyst as NiO [36]. Treatment of this sample in H_2 at 480°C, in situ, led to spectrum 14(b) which shows that most of the Ni near the surface was reduced to Ni metal [37]. The additional peaks to the left of the Ni metal peak in 14(b) are not well resolved but suggest that if unreduced Ni was present, it was different from most of that originally on the surface. Exposure of the reduced sample at 200°C to air, in situ, led to 14(c) which is similar to 14(a), although the left peak is not so well resolved, and indicates a reoxidation of the Ni. Spectrum 14(d) was obtained after a supported Ni sample was sulfied in an H_2/H_2S flow for 2 hours at 480°C. The binding energy of the S (2p) line was 158.4 eV, indicating (1,p.122) that most of the sulfur was present on the catalyst as sulfide ion and was not oxidized during exposure of the sample to air during transfer.

The Ni ($2p_{3/2}$) line in 14(d) seems to be split but has a splitting different from that for NiO. Interpretation of 14(d) is not possible since it is not known whether all the Ni was sulfided. It is important to note, however, that this spectrum does not resemble the "fingerprint" of NiO. Spectrum 14(e) shows a somewhat surprising result obtained from a sample which was reduced in H_2, evacuated to 10^{-6}torr, and then treated at 80°C for 16 hours in CO. It was assumed that this procedure would remove all the reduced nickel as $Ni(CO)_4$. Spectrum 14(e), however, shows that a considerable amount of unoxidized Ni was present even after exposure of the sample to air during transfer to the spectrometer. Apparently, a surface oxidation of the Ni particles during the evacuation step prevented the formation of $Ni(CO)_4$ and passivated the Ni surface to prevent complete oxidation of the Ni particles during exposure to air.

The spectra in Figure 14 demonstrate qualitatively how XPS can be used to follow the chemical state of a supported metal after various treatments. A more precise identification of the extra peaks left after reduction, 14(b), and a more detailed study of the left peak in 14(a) are topics of interest for future study.

C. Crystalline Oxides

In some catalysts, active sites result from a change in the coordination number of surface atoms. In an attempt to study the sensitivity of x-ray photoelectron spectroscopy to coordination number changes, we took spectra of the crystalline aluminosilicate minerals kaolinite, microcline,

and sillimanite. In kaolinite the Al is 6-coordinate, in microcline it is 4-coordinate, and in sillimanite half the aluminum is 6-coordinate and half is 4-coordinate. To within the limits of the charging correction, no differences in the Al (2p) spectra for the three samples were observed. A point charge calculation for sillimanite (38), assuming the formal charges for Al, Si and O gave a difference of 4 eV between the potential at the 6-coordinate Al site and the 4-coordinate Al site. Since no broadening of the 2.2 eV wide Al (2p) line was observed, an upper limit for the binding energy shift between the two types of aluminum in sillimanite is 1 eV. Because of the uncertainty of the surface conditions of the samples, the reason for the negative result of the sillimanite experiment cannot be determined. The result suggests, however, that shifts due to a change in coordination number in oxides are small and difficult to measure.

Another set of experiments was performed on FeV_2O_4 spinel catalysts. The lower curves (squares) in Figure 15 are for FeV_2O_4 unused, and the upper curves in that figure are for FeV_2O_4 after use as a catalyst for the dehydrogenation of cyclohexane at 425°C in a pulsed microreactor (39). Both samples were exposed to air before the spectra were taken at room temperature. If the lower spectrum is taken as the standard, the result of use of FeV_2O_4 as a catalyst and subsequent exposure to air is seen to be twofold. The vanadium lines shifted to higher binding energy while the oxygen lines split slightly and shifted to lower binding energy. The iron was unperturbed. The shift, rather than a broadening, of the lines indicates that the chemical changes caused by the treatment

affected a surface layer and not just the surface itself. The treatment did not cause a major change in the bulk, however, since the x-ray diffraction patterns of both samples were identical.

The activity of the catalyst has been found to decrease with use (40). The upper spectrum may, therefore, reflect chemical changes caused by aging of the catalyst at reaction conditions. In any case, the ability of the technique to indicate changes in the surface layers of crystalline oxides should prove useful in studies of both the activation and aging of such catalysts. With more accurate control of surface conditions, surface layer stoichiometry of mixed oxides and perhaps the nature of the surface defects can be studied.

Finally, a study of Eu exchanged zeolites was undertaken. Zeolites exchanged with trivalent rare earth cations are widely used catalysts. Although research has been carried out on the structural properties and the relation of rare earth exchange to the production of OH groups in the zeolites, few studies have been aimed at investigation of chemical changes of the rare earth cations as a function of treatment. The high internal surface area of zeolites makes them particularly well suited for catalyst experiments with XPS. Although the outer surface of the zeolite particles may differ from the "bulk" because of lattice termination, photoelectrons escaping from below the surface reflect the properties of a relatively well-defined, crystalline internal surface. Europium is also particularly well suited for these experiments because, as mentioned, the shifts between Eu^{2+} and Eu^{3+} are unusually large.

The Na forms of mordenite and Y-zeolite were exchanged with a 3-5 fold excess (over 100% exchange) of $Eu(NO_3)_3$ in aqueous solution (41). X-Ray diffraction patterns showed that a high degree of crystallinity was maintained after exchange. Quantitative analysis to determine the stoichiometry of the exchange was not done.

Eu_2O_3 was taken as a reference compound for this work. Figure 16 shows the Eu ($4d_{3/2}$) and ($4d_{5/2}$) lines of Eu_2O_3 at room temperature and at 175°C after 4 hours at 450°C in H_2, in situ. The spin-orbit splitting of 5.7 eV between the $4d_{3/2}$ - $4d_{5/2}$ levels is in agreement with the XPS results of Nilsson et al. (42). Most important is that there is no obvious difference between spectra (a) and (b) in Figure 16. Therefore, no significant changes in the surface layer of Eu_2O_3 occurred as a result of the reduction treatment. Reduction of the Eu zeolites is shown in Figure 17. The intensity ratio of the $4d_{3/2}$ - $4d_{5/2}$ lines of Eu^{3+} is obscured by the presence of the Mg, $K\alpha_{3,4}$ x-ray satellite peaks of the Si (2s) level. The presence of Eu^{2+} in the reduced samples is clear, however, and the measured shift of 7.6 eV is again in agreement with values of Nilsson et al. for the Eu^{3+} - Eu^{2+} shift. Reduction times were about 4 hours. As can be seen in spectrum 17(d), the reduction of $Eu^{3+}Y$ is at least partly reversible since treatment of the sample in O_2 at 80°C led to reoxidation of about half of the Eu^{2+}.

The difference in behavior between Eu_2O_3 and the Eu-zeolites can be accounted for by the properties of the zeolite. In most solids, the arrangement of atoms with respect to one another is determined by mutual

interactions. Cation exchanged zeolites are ususual in this respect. Since the alumino-silicate framework is relatively rigid, the exchange cations must adjust to the lattice as a function of treatment rather than vice versa. This adjustment can lead to unusual chemical environments for various cations and, further, can allow some unusual chemical reations.

Many rare-earth cations have trivalent states more stable than Eu^{3+}. Since zeolites are usually exchanged with a mixture of rare-earth ions, however, the observation of the reduction of the Eu^{3+} in zeolites suggests that further studies of the chemistry of rare-earths in zeolites may be useful in the understanding of zeolite activity.

V. CONCLUSIONS

The experiments presented in the previous section have been hampered by poor vacuum conditions and in some cases by inadequate calibration. In spite of these limitations, we feel that the utility of x-ray photoelectron spectroscopy to the study of chemical states on a variety of catalyst surfaces has been demonstrated. Nitrogen containing molecules adsorbed on zeolites have been observed and chemical shifts in the N (1s) line of NH_4Y zeolite as a function of temperature have been recorded. Spectra of supported Pt have shown effects of dispersion on the oxidizability of the Pt. Spectra of Eu^{3+} exchanged zeolites and supported Cu and Ni have given evidence of in situ reduction after treatment with hydrogen at elevated temperatures. Chemical changes in an oxide surface after use as a catalyst have also been observed.

On the basis of these results, we feel that x-ray photoelectron spectroscopy will find use in many important areas of catalyst research. Through measurement of chemical shifts and peak areas, studies of such subjects as catalyst characterization, activation, aging, and poisoning, as well as adsorption and surface segregation in multicomponent systems should be fruitful. In some cases, studies of alloys, homogeneous catalysts in frozen solutions and reactions of molecular beams at surfaces may also be possible. Low intensities and the relatively wide x-ray line make investigation of valence bands and the d-bands of very small metal particles difficult. The use of ultraviolet excitation of photoelectrons may be more fruitful in those cases.

The value of investigations of the type outlined above will, of course, depend on the extent to which the problems encountered in this research can be resolved. High rates of data accumulation and good control of the surface condition of the sample are imperative for XPS studies of catalysts. A more thorough study of shifts in known compounds and electron escape depths in solids would aid interpretation of data.

At this stage in the development of the technique, investigation of chemical effects involving large changes in the charge on atoms of interest have the best chance for success. More subtle chemical changes will become amenable to quantitative study with more accurate charging and band bending corrections and improved methods for dealing with the Fermi level energy reference for solids. X-Ray photoelectron spectroscopy is still developing rapidly, both experimentally and theoretically. We expect, therefore, that

the scope of applications of this technique to catalysis will continue to broaden.

Acknowledgements

Support of this work by the U. S. Atomic Energy Commission and an Air Force Office of Scientific Research Postdoctoral Research Award to W. N. D. is gratefully acknowledged. It is a pleasure to thank Professor David A. Shirley for his guidance through all phases of this research program. We thank Dr. T. Novakov (now at the Shell Development Co, Emeryville, California), Dr. J.M. Hollander and the remainder of the research group at the Field-Free Laboratory, Lawrence Radiation Laboratory, University of California, Berkeley, for assistance and many helpful discussions. We are indebted to B.R. Powell (now at the College of William and Mary, Williamsburg, Virginia), a student in the undergraduate summer research program at the Lawrence Radiation Laboratory, for carrying out the Eu experiments and to Dr. J.C. Helmer at Varian Associates, Palo Alto- California, for making his NiO data available to us. We also thank Drs. R. J. Houston, A. L. McClellan, J. Q. Adams and G. D. Christofferson at the Chevron Research Company, Richmond, California, Dr. R. L. Garten (now at the Esso Research and Engineering Company, Linden, New Jersey), A. B. Walters, G. Bergstrom (now at the Crown-Zellerbach Company, Camus, Washington) and Professor M. Boudart at Stanford University, Stanford, California, and Professor R. P. Merrill, R. M. Goodman and Professor G. A. Somorjai at the University of California, Berkeley, for donation and analysis of

many of the samples used in these experiments and for discussion of the results. Preparation of this manuscript has been supported by the Department of Engineering and Applied Science, Yale University. We thank Professors W. D. Robertson and D. E. Rosner of that Department for helpful comments on the manuscript.

References

1. K. Siegbahn, C. Nordling, A. Fahlman, R. Nordberg, K. Hamrin, J. Hedman, G. Johansson, T. Bergmark, S.-E. Karlsson, I. Lindgren and B. Lindberg, ESCA - Atomic, Molecular and Solid State Structure Studied by Means of Electron Spectroscopy: Nov. Act. Reg. Sci. Upsaliensis (IV), 20 (Almqvist and Wiksells, Uppsala, 1967).

2. J. M. Hollander, D. N. Hendrickson and W. L. Jolly, J. Chem. Phys. Communication, 49, 3315 (1968).

3. C. S. Fadley and D. A. Shirley, Phys. Rev. Letters, 14 980 (1968) and Rept. UCRL 18953 (Lawrence Radiation Laboratory, University of California, Berkeley 1970, to appear in N.B.S. J. Res.)

4. D. W. Turner, Chapter 3 in Physical Methods in Advanced Inorganic Chemistry, ed. by M. A. O. Hill and P. Day, Interscience Publishers, Inc., London (1968).

5. C. N. Berglund and W. E. Spicer, Phys. Rev., 136, A1030 and A1044 (1964).

6. W. T. Bordass and J. W. Linnett, Nature, 222, 660 (1969).

7. L. A. Harris, J. Appl. Phys., 39, 1419 (1968).

8. T. A. Carlson, M. O. Kranse, W. E. Moddeman, B. P. Pullen, and F. W. Ward, Physics Division Annual Progress Report, 1968 (Oakridge National Laboratories, Oakridge, Tennessee). D. Stalherm, B. Cleff, H. Hillig and W. Mehlhorn, Verhandl. DPC (VI), 4, 350 (1969).

9. C. S. Fadley, S. B. M. Hagström, M. P. Klein and D. A. Shirley, J. Chem. Phys., 48, 3779 (1968).

10. C. S. Fadley, G. L. Geoffroy, S. B. M. Hagström, and J. M. Hollander, Nucl. Inst. and Meth., 68, 177 (1969).

11. E. A. Stern and R. A. Ferrell, Phys. Rev., 120, 130 (1960); C. J. Powell and J. B. Swan, Phys. Rev., 118, 640 (1960).

12. C. J. Powell and J. B. Swan, Phys. Rev., 115, 869 (1959).

13. C. S. Fadley and C. Rugge, private communication. Recent work with this fitting procedure indicates that Lorentzian peaks with flat tails give the best fit to narrow peaks obtained from solids.

14. W. L. Jolly and D. N. Hendrickson, Rept. UCRL - 19050 (Lawrence Radiation Laboratory, University of California, Berkeley 1969).

15. T. Novakov and J. M. Hollander, Phys. Rev. Letters, 21, 1133 (1968).

16. T. Novakov and J. M. Hollander, Bull. Am. Phys. Soc., 14, 524 (1969).

17. J. Hedman, P.-F. Hedén, C. Nordling, and K. Siegbahn, Phys. Letters, 29A, 178 (1969).

18. C. S. Fadley, D. A. Shirley, A. J. Freeman, P. S. Bagus, J. V. Mallow, Phys. Rev. Letters, 23, 1397 (1969).

19. P. W. Palmberg and T. N. Rhodin, J. Appl. Phys., 39, 2425 (1968).

20. K. Højendahl, Kgl. Danske Videnskab. Selskab., Math, - fys. Medd., 16, 133 (1938).

21. J. C. Helmer, N. H. Weichert, Appl. Phys. Letters, 13, 266 (1968).

22. C. S. Fadley, C. E. Miner, and J. M. Hollander, Appl. Phys. Letters, 15, 223 (1969).

23. L. A. Harris, Surface Science, 15, 77 (1969).

24. R. P. Eischens, Science, 146, 486 (1964).

25. N. Svartholm and K. Siegbahn, Arkiv. f. Mat. Astr. Fys., 33A, 21 (1946).

26. C. S. Fadley, Ph.D. Thesis, University of California, Berkeley, 1970 (Rept. UCRL 19535 Lawrence Radiation Laboratory).

27. H. Heyne and F. C. Tompkins, Proc. Roy. Soc. [London], A292, 460 (1966).

28. Preparation and CO uptakes of samples done by R. J. Houston, Chevron Research Co., Richmond, California.

29. Sample supplied by G. Bergstrom and M. Boudart, Stanford University.

30. Samples supplied by A. B. Walters and M. Boudart, Stanford University.

31. J. V. Evans and T. L. Whateley, Trans. Faraday Soc., 63, 2769 (1967).

32. Samples prepared by A. L. McClellan, Chevron Research Company, Richmond, California.

33. W. J. Moore, Seven Solid States, Chapter V, W. A. Benjamin Inc., New York (1967).

34. Supplied by R. M. Goodman and Professor G. A. Somorjai, University of California, Berkeley.

35. J. C. Helmer, unpublished results.

36. An x-ray diffraction pattern of this sample accounted for about 30% of the total Ni in the form of NiO crystallites with an average size of about 120Å.

37. An x-ray diffraction pattern of a reduced sample accounted for about 60% of the total Ni in the form of metallic Ni crystallites with an average size of about 140Å and gave no evidence of NiO.

38. J. Q. Adams and T. R. Hughes, unpublished results.

39. Samples supplied by Professor R. P. Merrill, University of California, Berkeley.

40. T. P. Seider, G. J. F. Breedveld, and R. P. Merrill, unpublished results.

41. Experimental work carried out by B. R. Powell, as part of the Lawrence Radiation Laboratory undergraduate summer research program.

42. O. Nilsson, C.-H. Nordberg, J.-E. Bergmark, A. Fahlman, C. Nordling, and K. Siegbahn, Helv. Phys. Acta., 41, 1064 (1968).

Figure Captions

Figure 1. Nitrogen (1s) binding energies vs. charge on the nitrogen atom calculated by the Complete Neglect of Differential Overlap, molecular orbital method (2). Compounds are identified in Table 1.

Figure 2. Iodine $3d_{5/2}$ photoelectron lines from 1, 3, and 10 double layers of α-iodostearic acid (1, p.140 - by permission of Nova Acta Reg. Soc. Sc. Upsaliensis).

Figure 3. O (1s) and Fe (3p) photoelectron lines from iron foil at various temperatures in a low pressure of H_2 (3).

Figure 4. Partial photoelectron spectra from Y zeolite and Mordenite.

Figure 5. Schematic representation of energy levels in a solid sample in a photoelectron spectrometer (9).

Figure 6. Schematic diagram of the Berkeley, 50 cm, iron-free, magnetic x-ray photoelectron spectrometer (9).

Figure 7. I ($3d_{5/2}$) and C (1s) photoelectron lines from gas phase CH_3I. Left spectra taken with an Mg anode, right spectra with an Al anode.

Figure 8. N (1s) photoelectron lines from NH_4-Y zeolite as a function of treatment <u>in situ</u>.

Figure 9. Pt($4f_{5/2}$) and ($4f_{7/2}$) photoelectron lines from various Pt samples.

Figure 10. Pt($4f_{5/2}$) and ($4f_{7/2}$) photoelectron lines from 1% Pt on graphon as a function of treatment.

Figure 11. C (1s) photoelectron from MgO and 5% Cupric acetate on MgO.

Figure 12. Cu($2p_{3/2}$) photoelectron lines from various copper samples.

Figure 13. Ni($2p_{3/2}$) photoelectron lines from NiO and nickel metal.

Figure 14. Ni($2p_{3/2}$) photoelectron lines from 6% Ni on silica-alumina.

Figure 15. Partial photoelectron spectra from FeV_2O_4 before (squares) and after (dots) use as a catalyst for the dehydrogenation of cyclohexane at 425°C.

Figure 16. Eu ($4d_{3/2}$) and ($4d_{5/2}$) photoelectron lines from Eu_2O_3 at room

temperature and at 175°C after heating in H_2 to 450°C *in situ*.

Figure 17 Eu ($4d_{3/2}$) and ($4d_{5/2}$) photoelectron lines of Eu exchanged mordenite and Y zeolite as a function of treatment *in situ*.

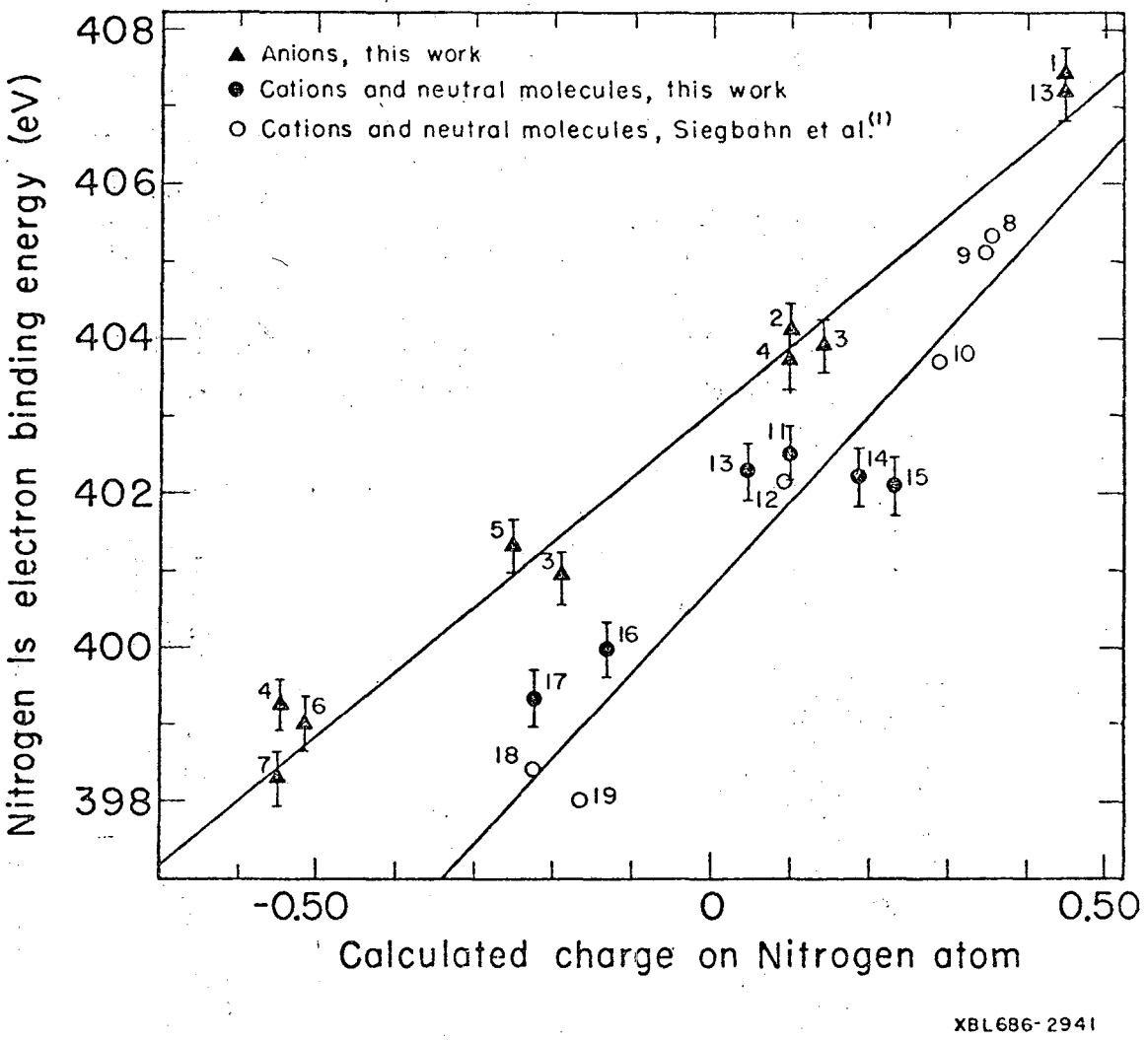
▲ Anions, this work
● Cations and neutral molecules, this work
○ Cations and neutral molecules, Siegbahn et al.[1]
Nitrogen 1s electron binding energy (eV)
408
406
404
402
400
398
-0.50
0
0.50
Calculated charge on Nitrogen atom
XBL686-2941

Figure 1

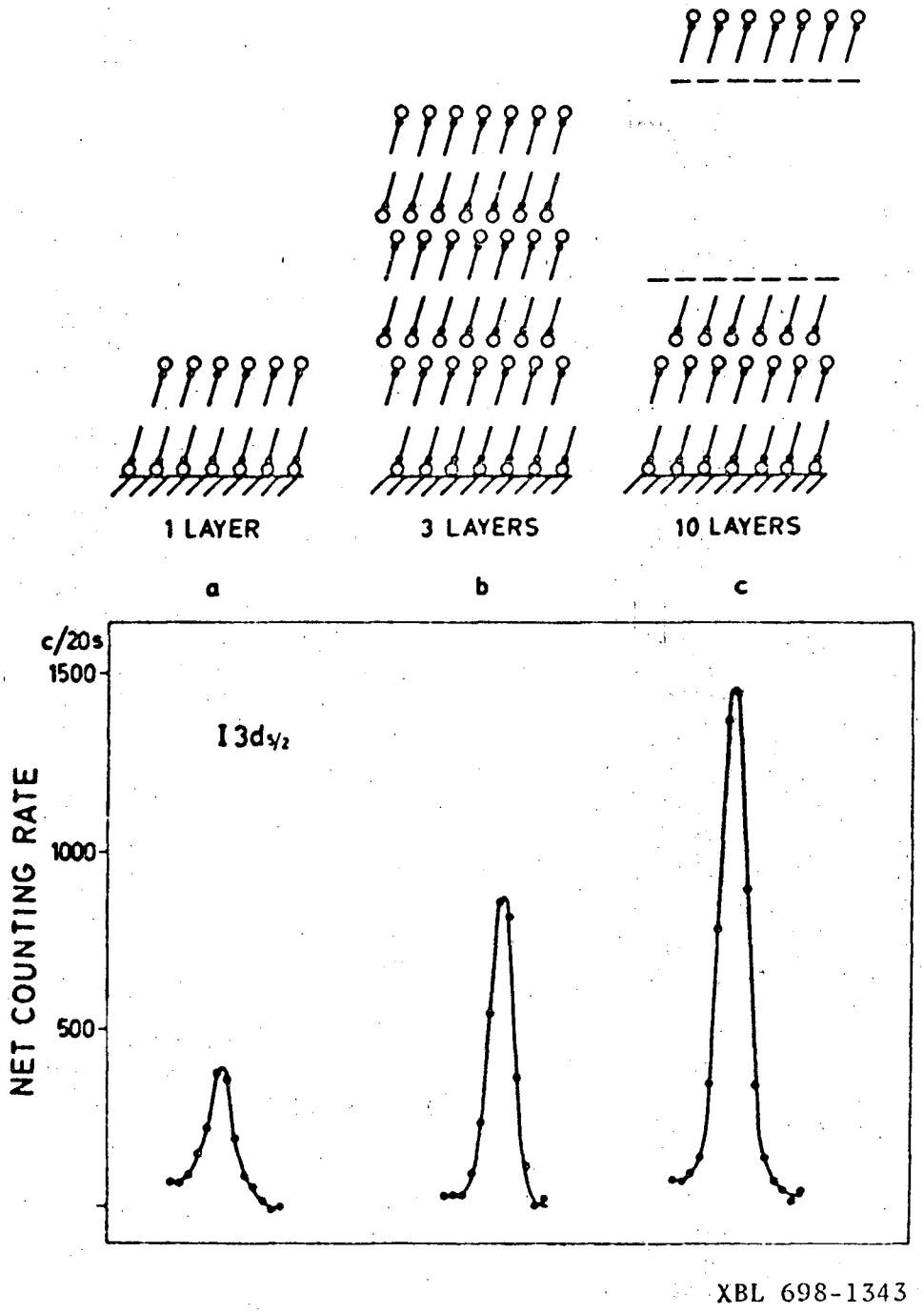

XBL 698-1343

Figure 2

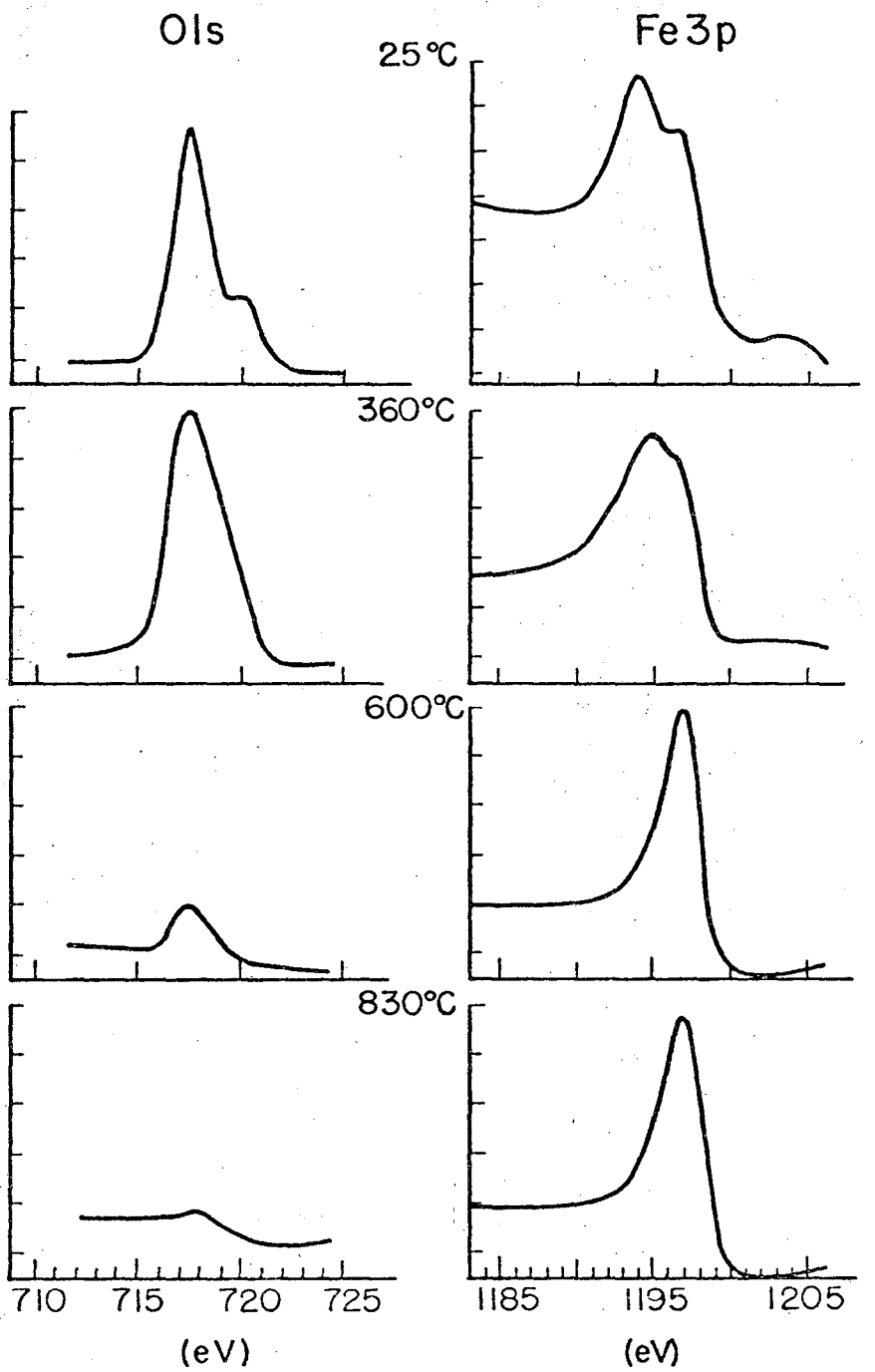
O1s
Fe3p
25°C
360°C
600°C
830°C
710
715
720
725
(eV)
1185
1195
1205
(eV)
XBL687-3421

Figure 3

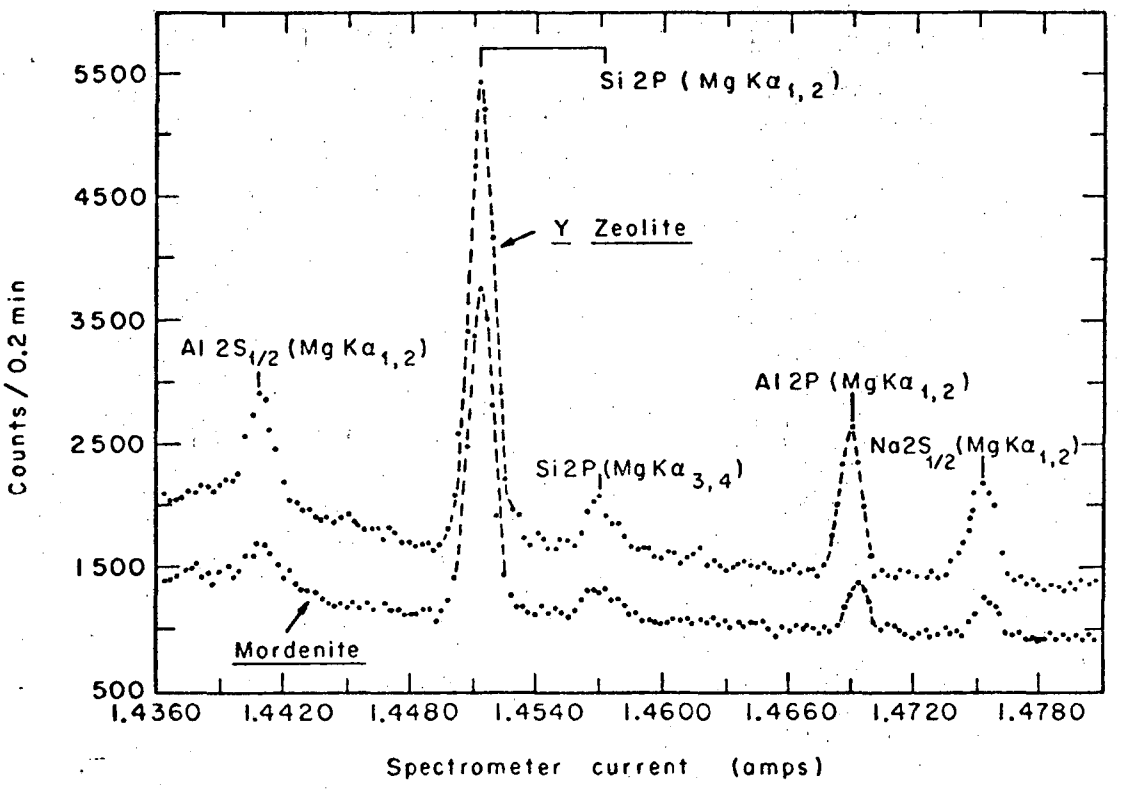
Si 2P (Mg Kα 1, 2)
Y Zeolite
Al 2S1/2 (Mg Kα 1, 2)
Al 2P (MgKα 1, 2)
Si 2P (Mg Kα 3, 4)
Na2S1/2 (Mg Kα 1, 2)
Mordenite
Counts / 0.2 min
5500
4500
3500
2500
1500
500
1.4360
1.4420
1.4480
1.4540
1.4600
1.4660
1.4720
1.4780
Spectrometer current (amps)
XBL694-2432

Figure 4

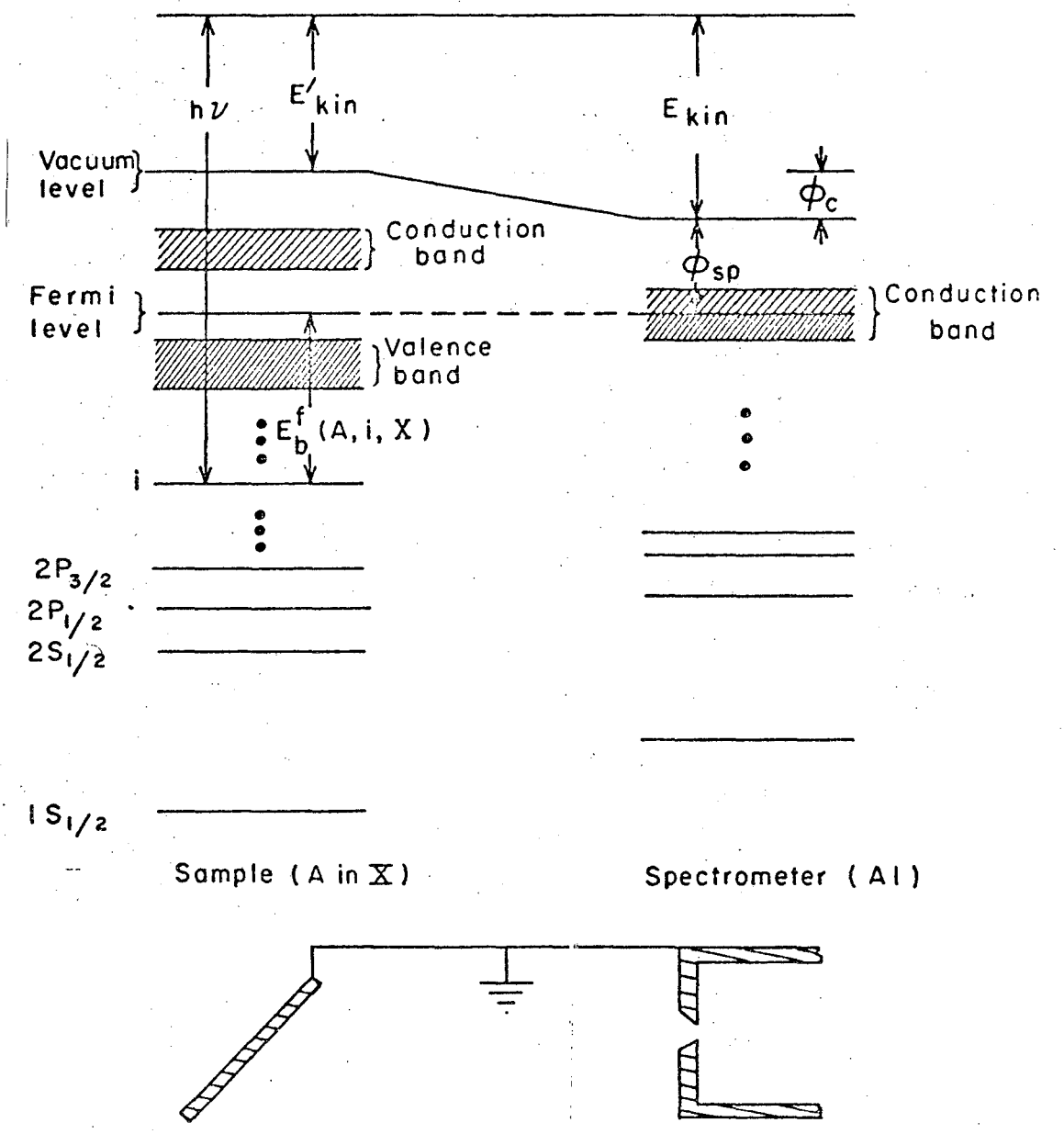

MUB-13959-A

Figure 5

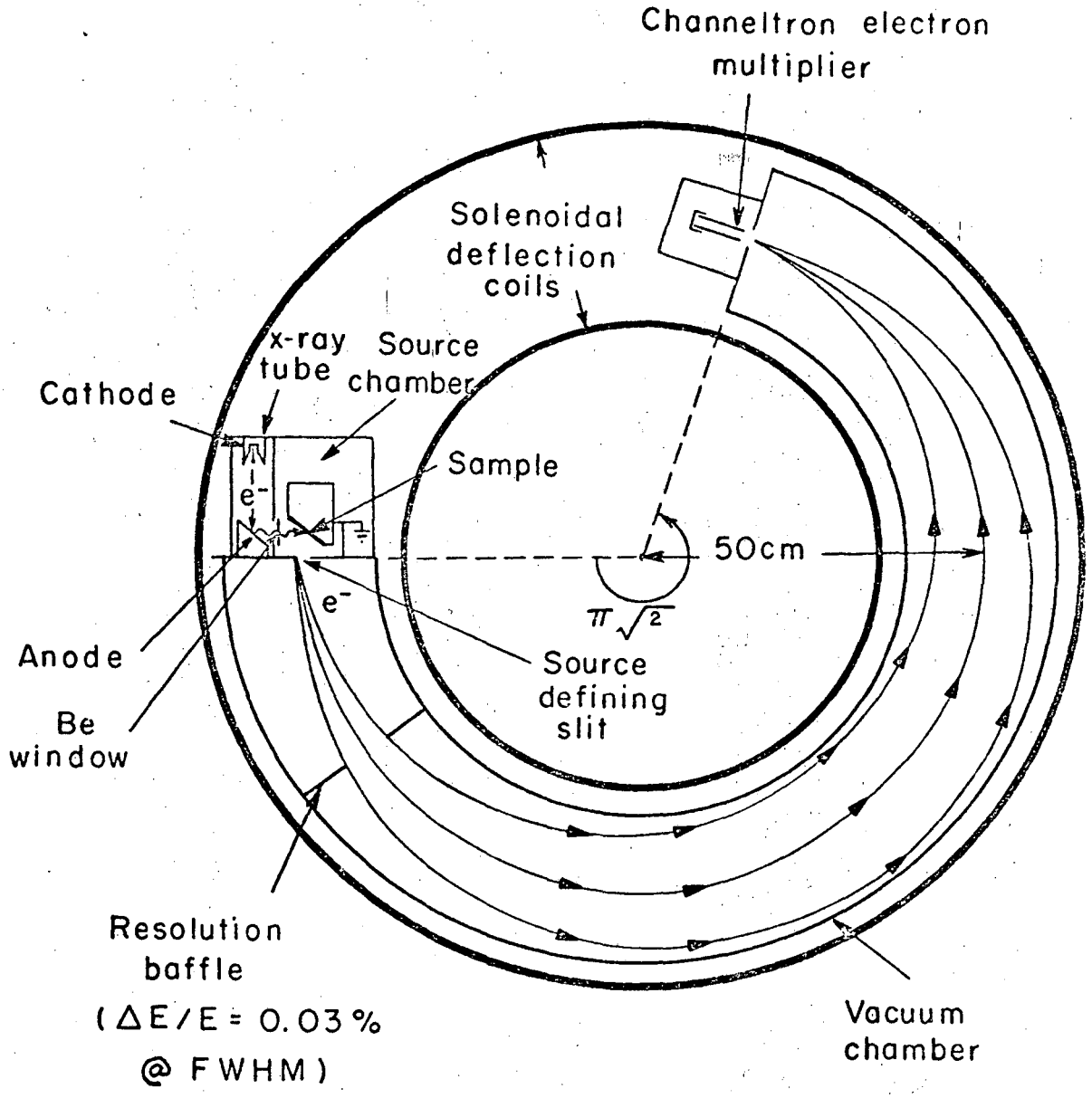

XBL694-2402

Figure 6

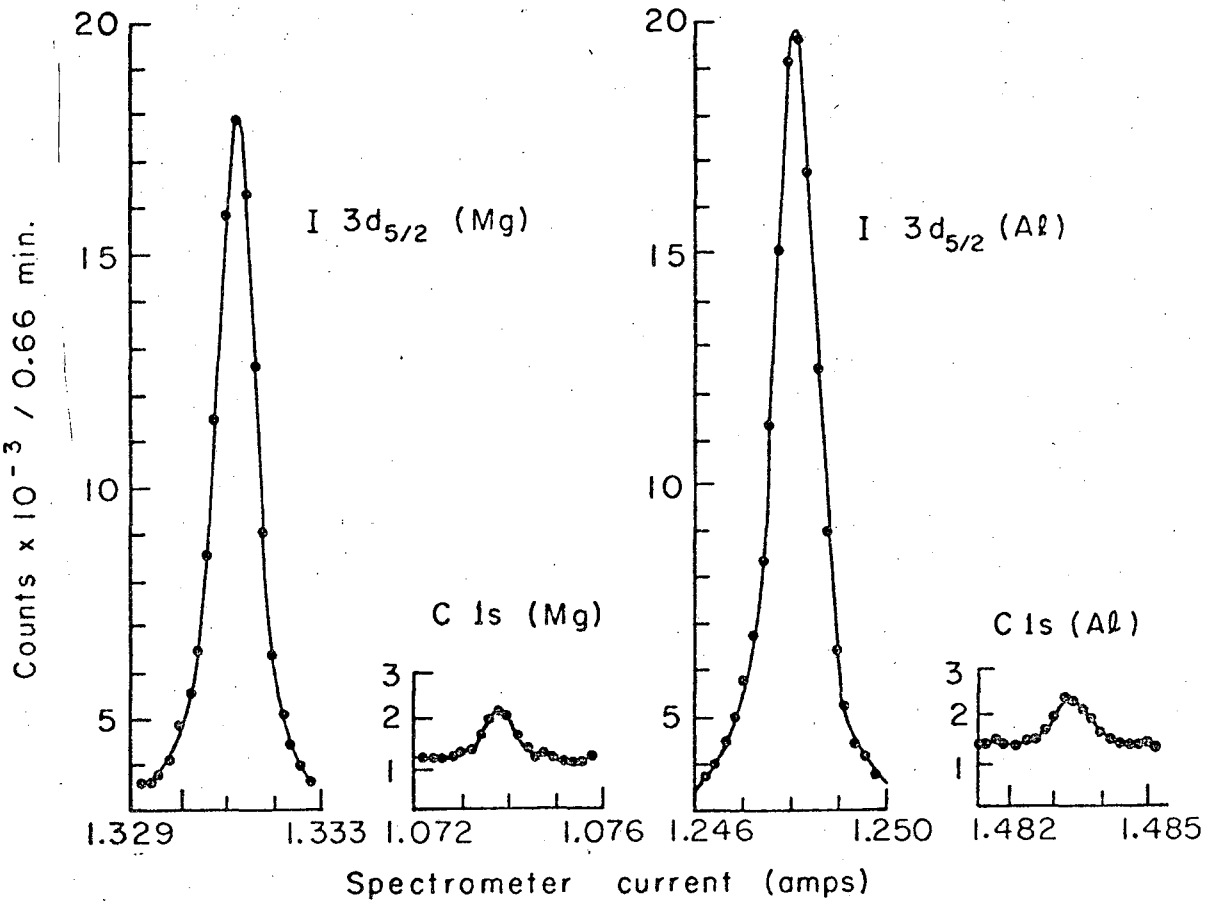

XBL 699-3713

Figure 7

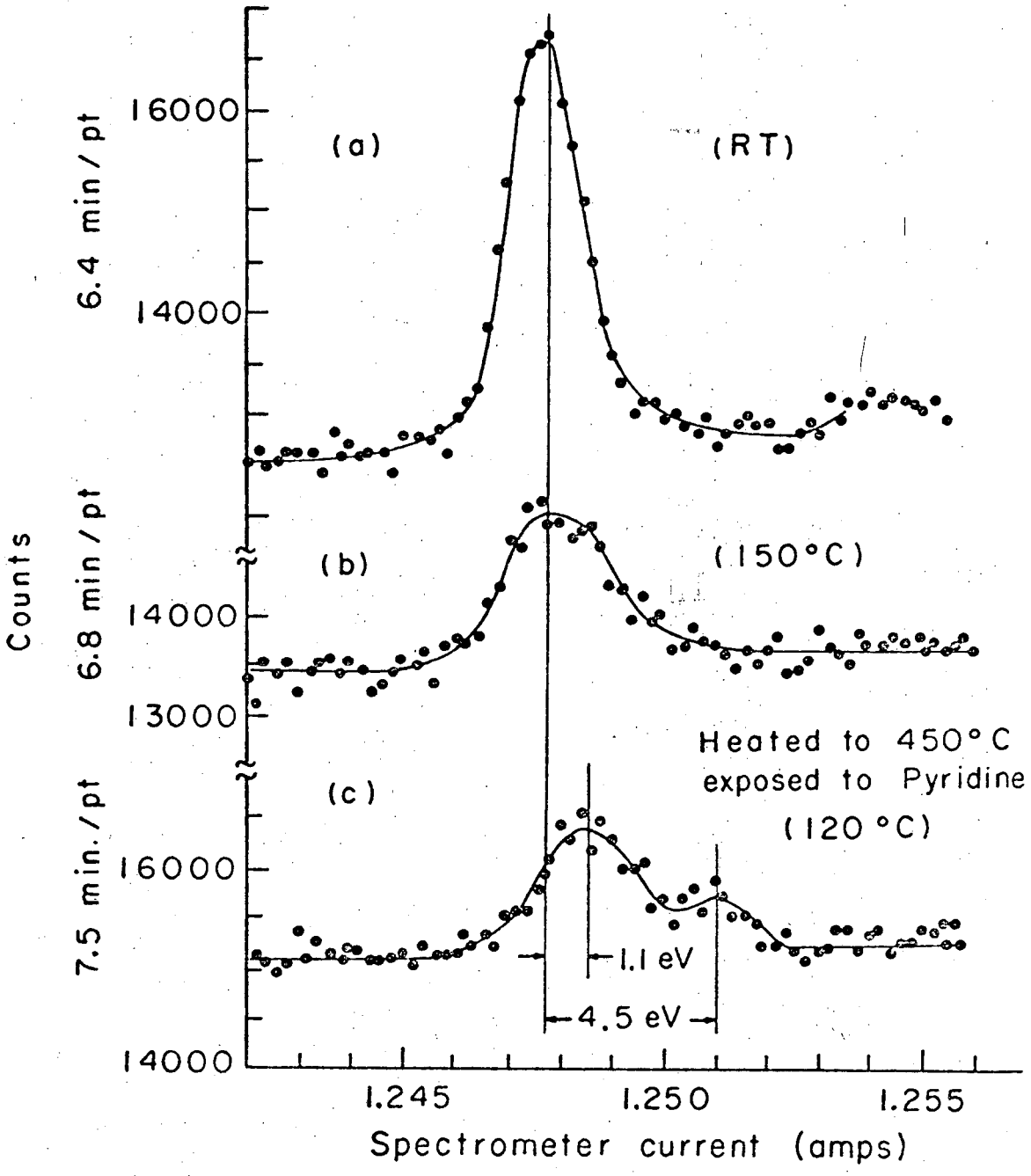
16000
14000
6.4 min / pt
(a)
(RT)
Counts
14000
13000
6.8 min / pt
(b)
(150°C)
Heated to 450°C
exposed to Pyridine
(120 °C)
16000
14000
7.5 min. / pt
(c)
1.1 eV
4.5 eV
1.245
1.250
1.255
Spectrometer current (amps)
XBL699-3709

Figure 8

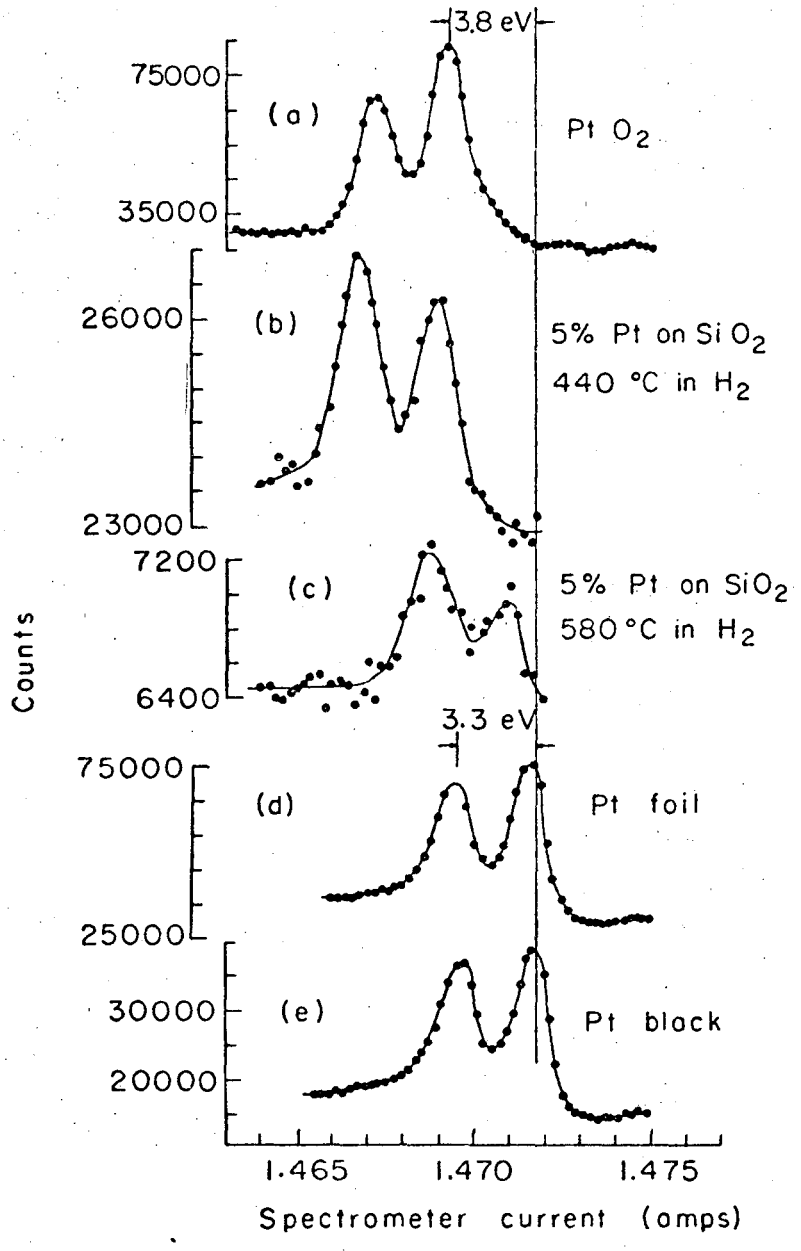
3.8 eV
75000
35000
(a)
Pt O2
26000
23000
(b)
5% Pt on Si O2
440 °C in H2
7200
6400
(c)
5% Pt on SiO2
580 °C in H2
Counts
3.3 eV
75000
25000
(d)
Pt foil
30000
20000
(e)
Pt black
1.465
1.470
1.475
Spectrometer current (amps)
XBL699-3705

Figure 9

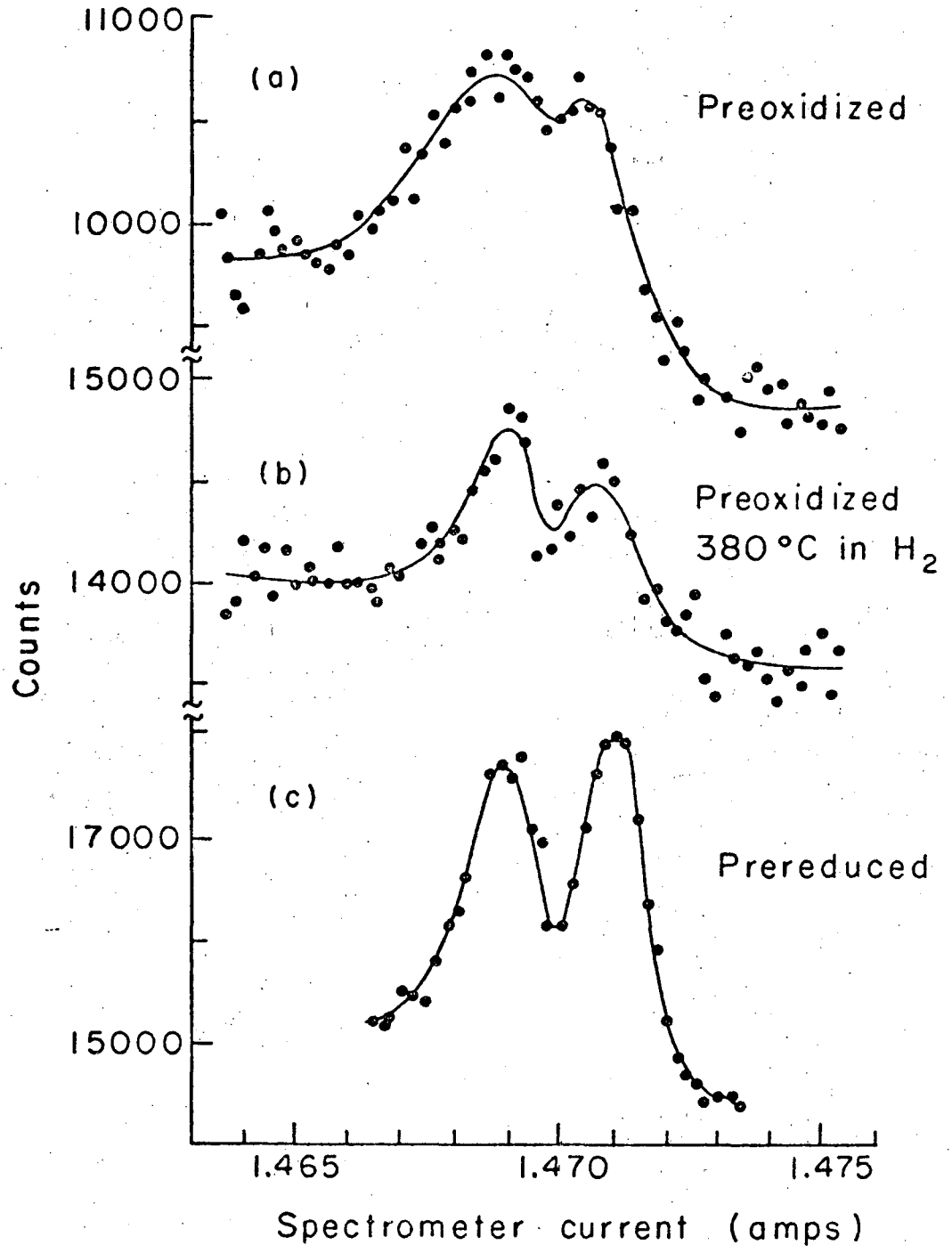
11000
10000
15000
14000
17000
15000
Counts
(a)
Preoxidized
(b)
Preoxidized
380 °C in H_2
(c)
Prereduced
1.465
1.470
1.475
Spectrometer current (amps)
XBL699-3710

Figure 10

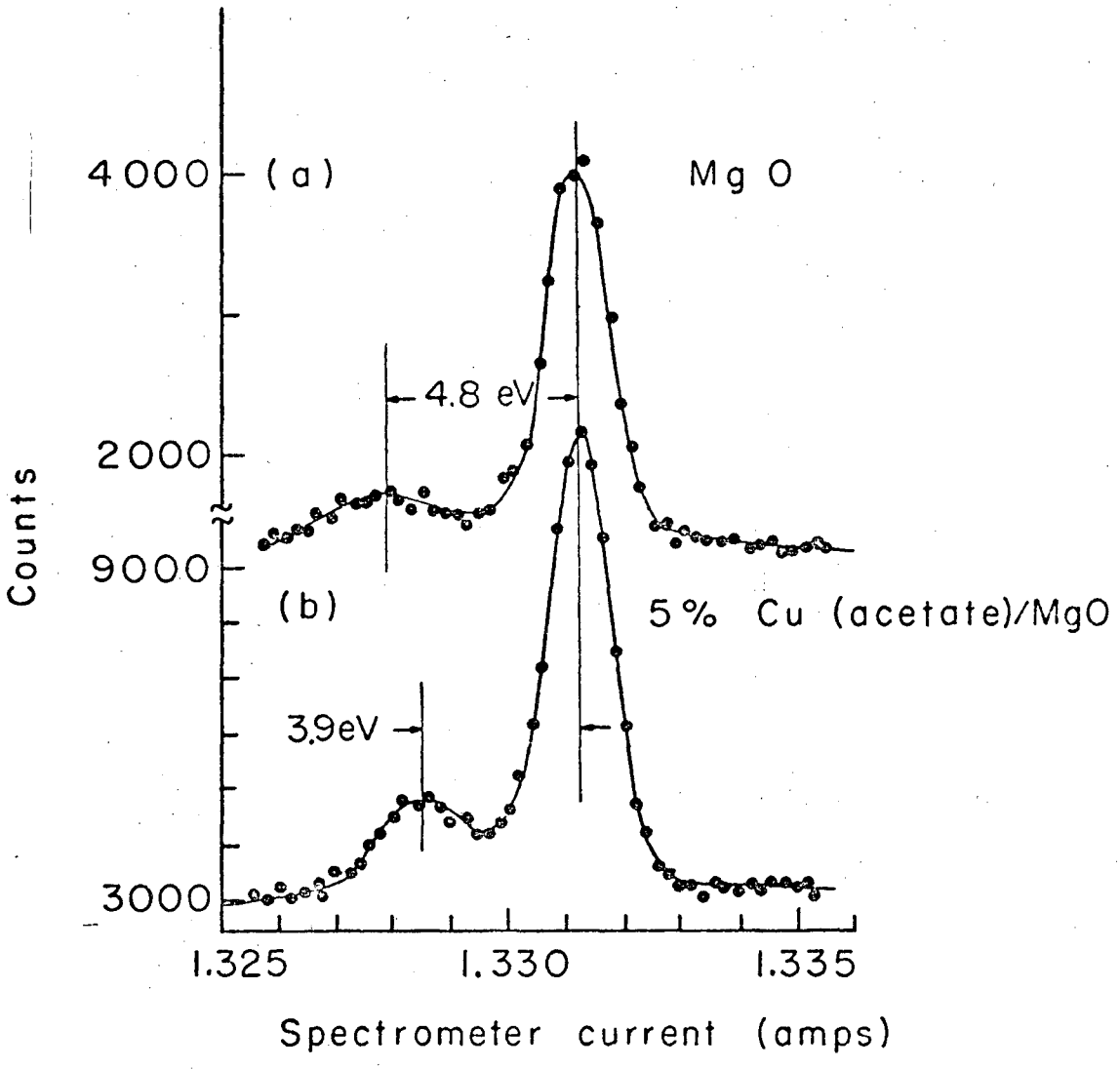
4000
(a)
Mg O
4.8 eV
2000
Counts
9000
(b)
5% Cu (acetate)/MgO
3.9eV
3000
1.325
1.330
1.335
Spectrometer current (amps)
XBL699-3712

Figure 11

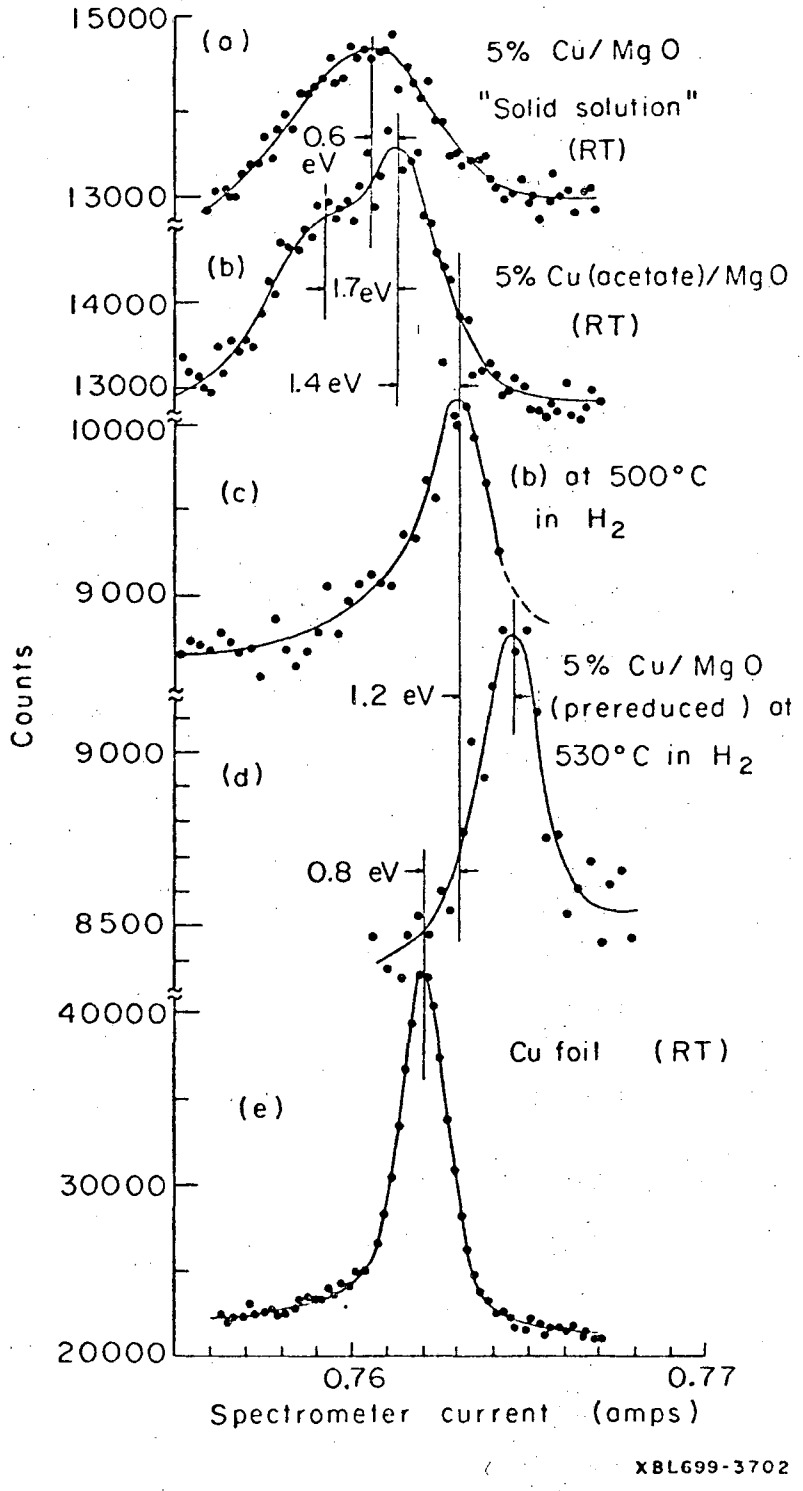
15000
(a)
5% Cu/MgO
"Solid solution"
(RT)
0.6 eV
13000
(b)
1.7eV
5% Cu(acetate)/MgO
(RT)
14000
13000
1.4 eV
10000
(c)
(b) at 500°C
in H2
9000
Counts
5% Cu/MgO
(prereduced) at
530°C in H2
1.2 eV
9000
(d)
0.8 eV
8500
40000
Cu foil (RT)
(e)
30000
20000
0.76
0.77
Spectrometer current (amps)
XBL699-3702

Figure 12

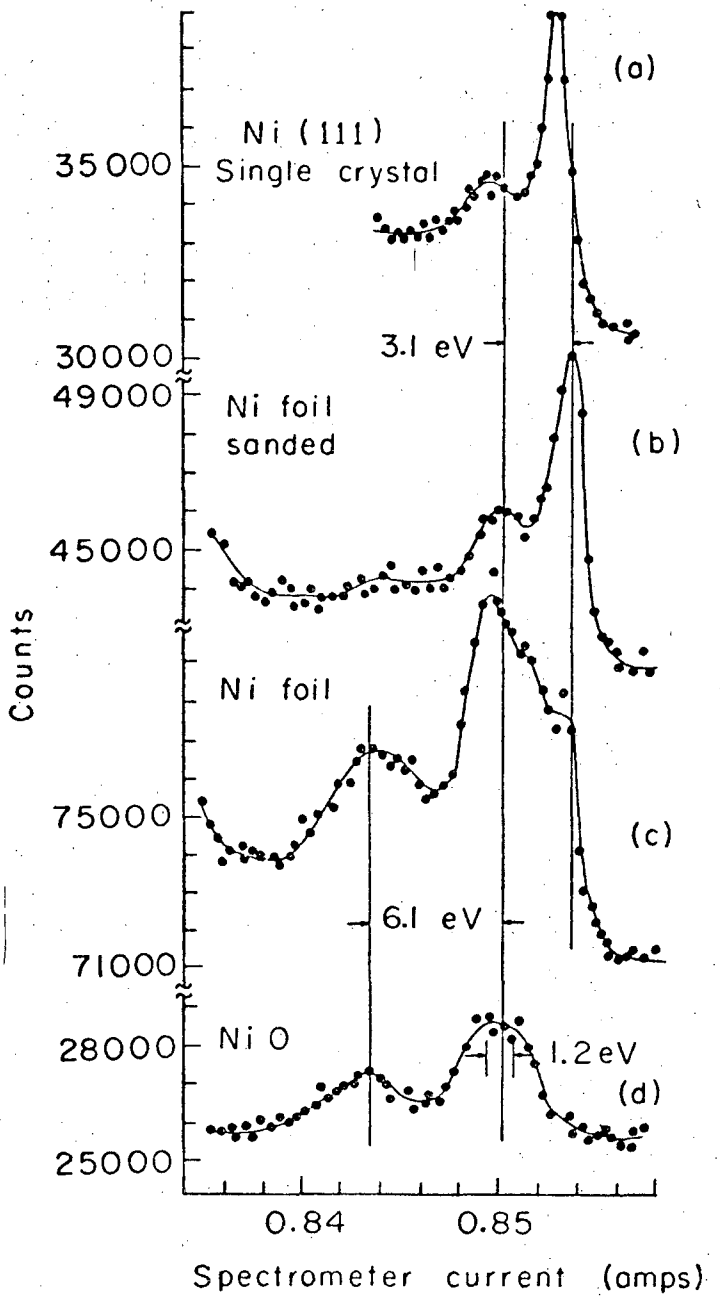

XBL699-3704

Fig. 13

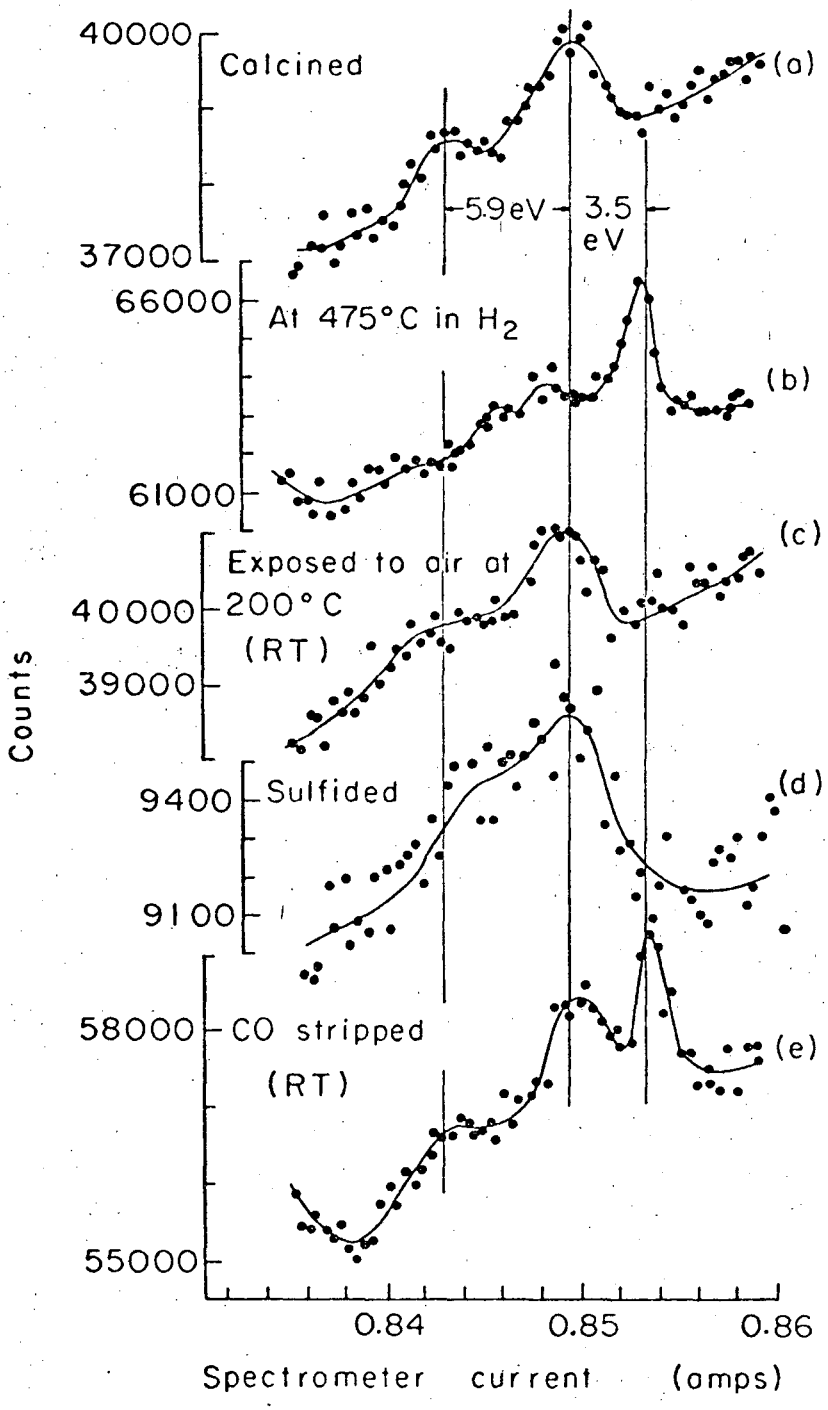
40000
Calcined
(a)
5.9eV
3.5 eV
37000
66000
At 475°C in H_2
(b)
61000
Exposed to air at 200°C (RT)
(c)
40000
39000
Counts
9400
Sulfided
(d)
9100
58000
CO stripped (RT)
(e)
55000
0.84
0.85
0.86
Spectrometer current (amps)

XBL699-3703

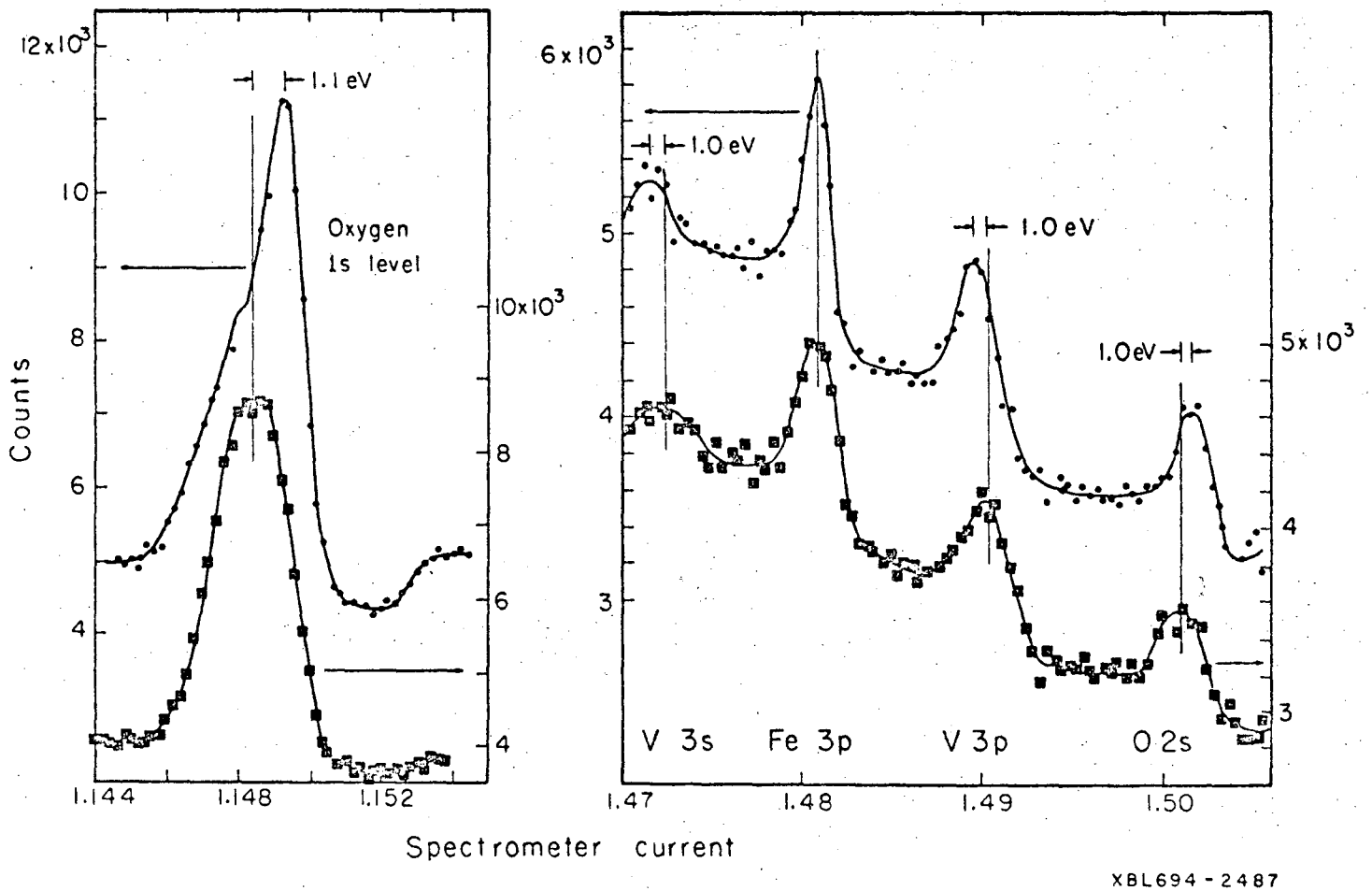
12x10³
10
8
6
4
1.1 eV
Oxygen
1s level
Counts
10x10³
8
6
4
1.144
1.148
1.152
6x10³
5
4
3
1.0 eV
1.0 eV
1.0eV
5x10³
4
3
V 3s
Fe 3p
V 3p
O 2s
1.47
1.48
1.49
1.50
Spectrometer current
XBL694-2487

FIGURE 15

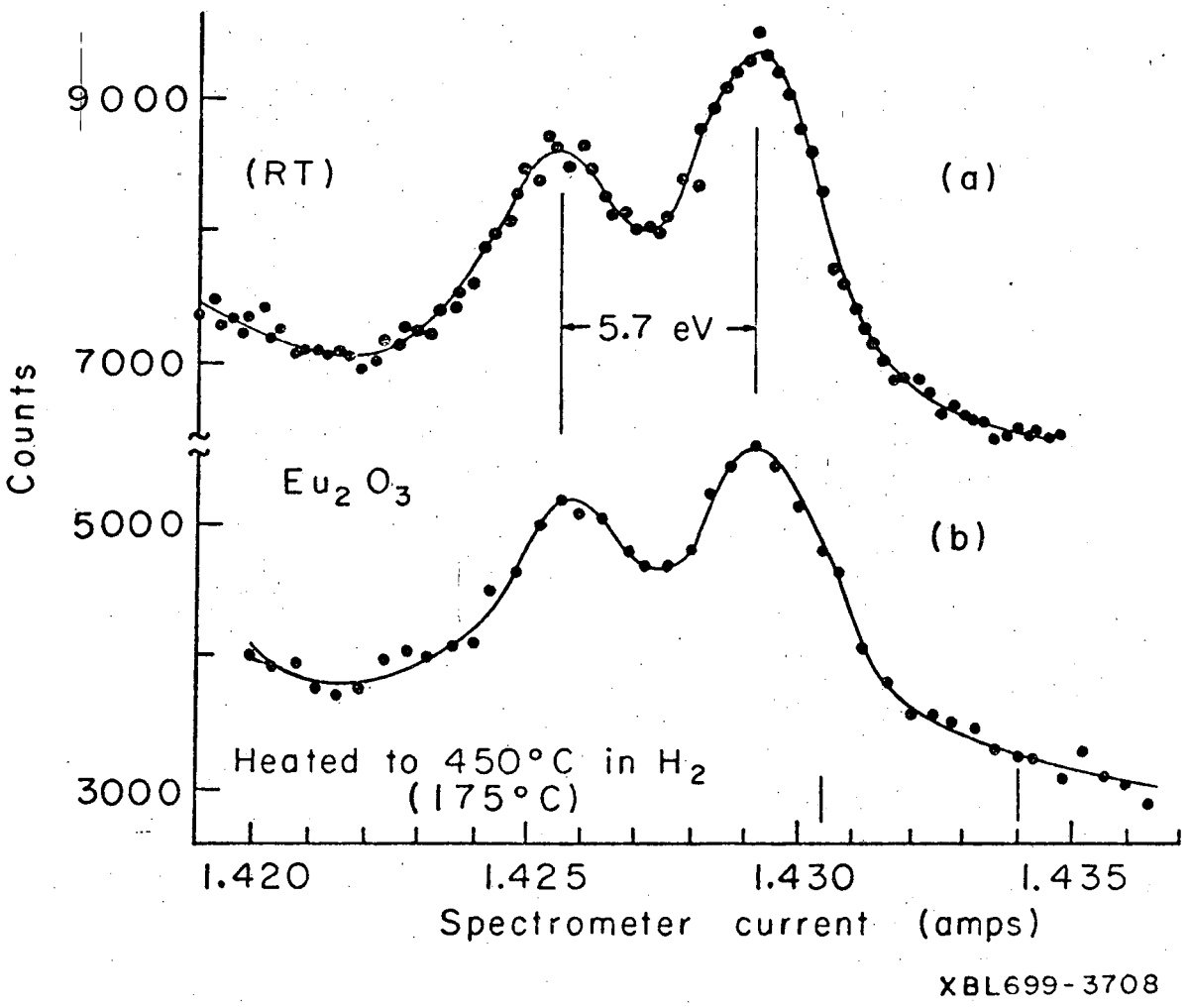
9000
7000
5000
3000
Counts
(RT)
(a)
5.7 eV
Eu_2O_3
(b)
Heated to 450°C in H_2
(175°C)
1.420
1.425
1.430
1.435
Spectrometer current (amps)
XBL699-3708

Figure 16

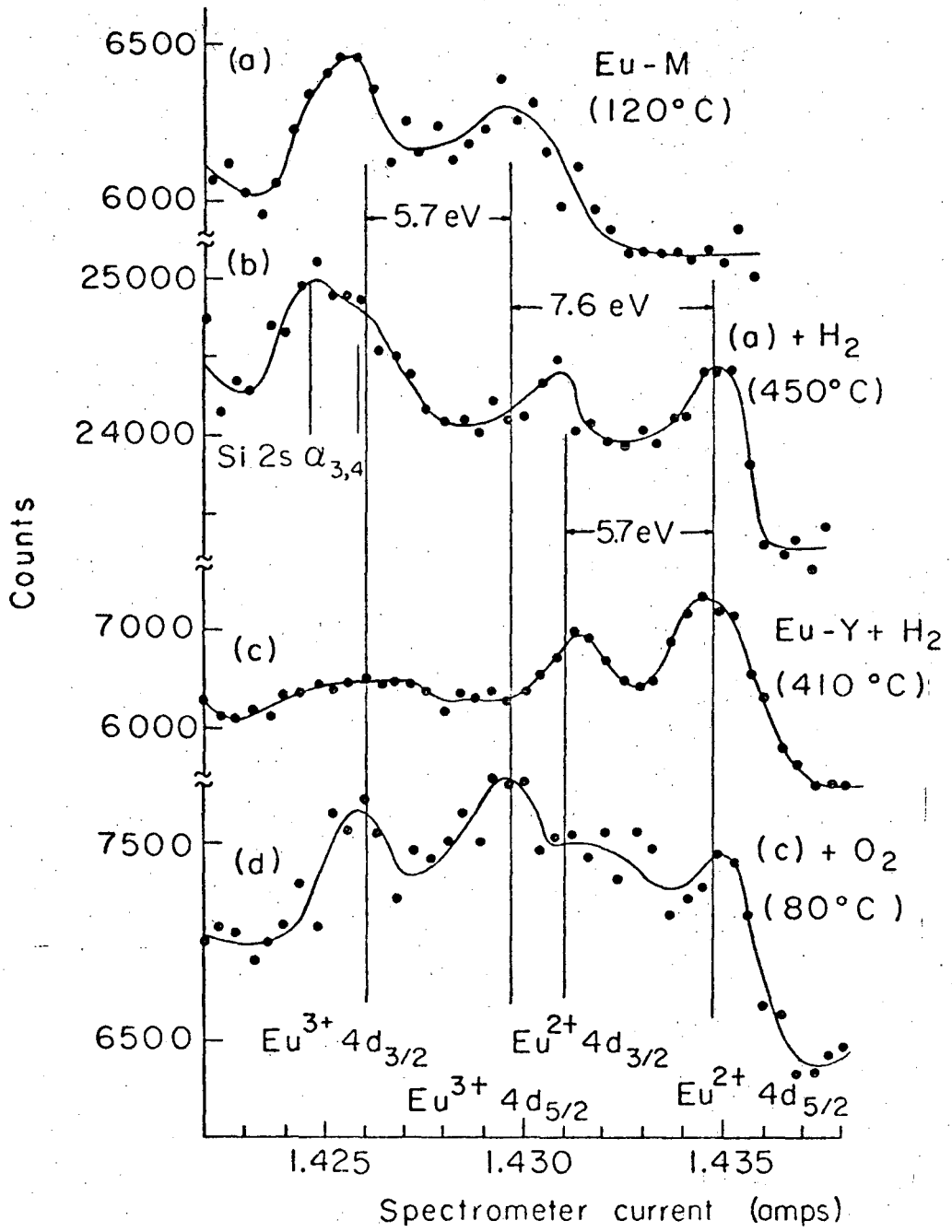

XBL699-3707

Figure 17